The Astrophysical Journal, 808:8 (21pp), 2015 July 20 doi:10.1088/0004-637X/808/1/8

MANY-BODY FORCES IN THE EQUATION OF STATE OF HYPERONIC MATTER

R. O. Gomes[1,2], V. Dexheimer[3], S. Schramm[2], and C. A. Z. Vasconcellos[1,4]
[1] Instituto de Física, Universidade Federal do Rio Grande do Sul, Porto Alegre, RS 91501-970 Brazil
[2] Frankfurt Institute for Advanced Studies, D-60438 Frankfurt am Main, Germany; rosana.gomes@ufrgs.br
[3] Department of Physics, Kent State University, Kent, OH 44242, USA
[4] ICRANet, Piazza della Repubblica 10, I-65122 Pescara, Italy
Received 2014 December 3; accepted 2015 May 22; published 2015 July 14

ABSTRACT

In this work we introduce an extended version of the formalism proposed originally by Taurines et al. that considers the effects of many-body forces simulated by nonlinear self-couplings and meson–meson interaction contributions. In this extended version of the model, we assume that matter is at zero temperature, charge neutral, and in beta-equilibrium, considering that the baryon octet interacts by the exchange of scalar–isoscalar (σ, σ^*), vector–isoscalar (ω, ϕ), vector–isovector (ϱ), and scalar–isovector (δ) meson fields. Using nuclear matter properties, we constrain the parameters of the model that describe the intensity of the indirectly density dependent baryon–meson couplings to a small range of possible values. We then investigate asymmetric hyperonic matter properties. We report that the formalism developed in this work is in reasonable agreement with experimental data and also allows for the existence of massive hyperon stars (with more than 2 $M_\odot$) with small radii, compatible with astrophysical observations.

Key words: dense matter – equation of state – stars: interiors – stars: neutron

1. INTRODUCTION

In the last decades, the determination of the equation of state (EOS) of nuclear matter at high densities has become one of the main goals of nuclear astrophysics. Experimental nuclear data together with neutron star observational measurements can and should be used to restrict the parameters of the models used to describe the EOS of neutron stars, not only at low, but also at high densities. For example, Schaffner-Bielich (2008) showed that hypernuclear data impose contraints in the composition of hyperon stars (see also references cited in Schaffner-Bielich 2008). More specifically, observations of 2 $M_\odot$ neutron stars (Demorest et al. 2010; Antoniadis et al. 2013) constrain the EOS of neutron stars, in particular its stiffness in the high density regime. A theoretical study that calculates the radii of 1.4 $M_\odot$ neutron stars also discusses the role played by matter above saturation density on neutron star properties (Fortin et al. 2014). Such compact stars are considered *canonical stars* because the most accurate mass measurement from the binary pulsar system PSR 1913+16, predicts masses of $1.3867 \pm 0.0002\,M_\odot$ and $1.4414 \pm 0.0002\,M_\odot$ (Lattimer & Prakash 2005; Weisberg & Taylor 2005).

Although the fundamental physics has to be described in terms of quarks and gluons, at scales of energy where only the baryon degrees of freedom are relevant, the residuum of the strong interaction between quarks can be described by effective hadronic models. The first attempts to describe the properties of nuclear matter were made in the 1950s, with the works of Johnson & Teller (Johnson & Teller 1955), which introduced classical nuclear potentials whose quanta were π mesons, and of Duerr (Duerr 1956), which reformulated this previous formalism in a relativistic approach, able to explain spin–orbit coupling. These two works were the seeds of a particular class of models, denominated relativistic mean field (RMF) models, in which the nuclear interaction is usually described by the exchange of scalar–isoscalar and vector–isoscalar mesons with minimal Yukawa coupling in a quantum field theory approach. These terms represent the attractive and repulsive components of the nuclear force in the long and short range regimes, respectively.

The first RMF model for nuclear matter was proposed in 1974 by Walecka et al. (Serot & Walecka 1986), introducing the description of nuclear matter in the exchange of scalar and vector mesons. This model, however, was not able to reproduce correctly the compressibility modulus of nuclear matter and the nucleon effective mass at saturation. As a consequence, several extensions of the model were developed in order to overcome the problem. Boguta and Bodmer proposed additional terms in the scalar sector by taking into account the nonlinear third and fourth orders of the σ meson self-interaction terms. With this, they could simulate field-dependent correlations in the in-medium nucleon–nucleon interaction (Boguta & Bodmer 1977). In later works, this same feature was extended to the ω meson (Sugahara & Toki 1994; Toki et al. 1995) and the case with crossed scalar–vector interaction terms was also investigated (Todd-Rutel & Piekarewicz 2005; Kumar et al. 2006). The meson–baryon coupling was also modified in other models, such as the ZM models with a derivative coupling (Zimanyi & Moszkowski 1990) and the density dependent meson–baryon coupling model proposed in Typel & Wolter (1999), as an alternative to the minimal coupling proposed by Walecka.

In particular, the models introduced by the works in Zimanyi & Moszkowski (1990) and Delfino et al. (1995a, 1995b) replace the Yukawa coupling $g_\sigma \overline{\psi}\sigma\psi$ by a derivative coupling $(g_\sigma \sigma/M)\overline{\psi}\gamma_\mu \partial^\mu \psi$ in a class of models denominated derivative scalar coupling models (DSCM). These models are Lorentz invariant but not renormalizable, and present the important features of a field dependence in the baryon–meson coupling, introducing an indirect density

dependence. Also the nonlinear terms for the scalar fields can be interpreted as many-body forces contributions. The DSCM were widely applied to study the bulk properies of nuclear matter (Choudhury & Rakshit 1993; Delfino et al. 1995a; Aguirre et al. 1996; Bhattacharyya & Raha 1996), finite nuclei (Biro & Zimanyi 1997; Chiapparini et al. 1997), hypernuclear matter (Barranco et al. 1991; Lombard et al. 1995), neutron stars (Glendenning et al. 1992), and also quark–meson coupling models (Aguirre & Schvellinger 1997) and beyond mean field approaches (Aguirre 2001). Finally, some attempts to introduce theoretical fundaments to the DSCM are presented in Miyazaki (1994), in which it is shown that such models are related to SU(6) model for the meson–baryon couplings, and also in Miyazaki (1995), in which results show similarities between a DSCM based approach and Dirac–Brueckner–Hartree–Fock theory.

Since the characteristic timescale for the population of neutron stars is long compared to the typical weak-interaction timescale, strangeness is not conserved in their interiors, for the appearance of net strangeness, which means hyperonic degrees of freedom. The topic of hyperons in neutron stars has been extensively discussed in the literature. In particular, the discussion relating new degrees of freedom to the softening of the EOS and, consequently, to the lowering of neutron stars maximum masses received renewed attention (Sahakian & Vartanian 1963; Glendenning 1982, 1985; Knorren et al. 1995; Hanauske et al. 2000; Schaffner-Bielich et al. 2002) due to the observations of massive neutron stars. However, as first shown in (Schaffner & Mishustin 1996), this problem is avoided by the addition of the pair of strange mesons σ^* and ϕ (associated, respectively, to $f_0(975\ \mathrm{MeV})$ and $\phi(1020\ \mathrm{MeV})$; Beringer et al. 2012), where the latter one introduces a new repulsion to the interaction of hyperons. Although additional uncertainties concerning the hyperonic coupling are added to the formalism (Fortin et al. 2014), in the presence of these additional mesons, several authors succeeded in describing massive hyperon stars using different models (Dexheimer & Schramm 2008; Bednarek et al. 2012; Bonanno & Sedrakian 2012; Lastowiecki et al. 2012; Weissenborn et al. 2012a, 2012b; Banik et al. 2014; Bhowmick et al. 2014; Gusakov et al. 2014; Lopes & Menezes 2014b; van Dalen et al. 2014; Yamamoto et al. 2014).

The formulation used in this work is based on the model proposed in Taurines et al. (2001) as an attempt to unify the Walecka and ZM models in a general fashion. This formalism considers a parametric derivative coupling that simulates the many-body forces by including nonlinear self-interaction and meson–meson interaction terms for the scalar mesons in the Lagrangian density of the theory. The meson–baryon couplings are implicitly density dependent and parametrized by a constant. The parametric coupling formalism reproduces successfully nuclear matter properties and has been applied to investigate different topics related to nuclear physics, such as the nuclear matter compressibility (Dexheimer et al. 2008), hadron-quark phase transitions (Burigo et al. 2010), kaon condensation (Razeira et al. 2011), symmetry energy (Marranghello et al. 2010), and effects of magnetic fields on neutron stars (Gomes et al. 2014a, 2014b).

In this work, we present an extended version of the parametric model including the entire set of mesons relevant to the scale of energy and mean field approximation: scalar–isoscalar (σ, σ^*), vector–isoscalar (ω, ϕ), vector–isovector (ϱ), and scalar–isovector (δ) meson fields. The ϱ and δ mesons are very important for the description of neutron stars, as these are highly isopin asymmetric objects (Kubis & Kutschera 1997; Liu et al. 2002; Menezes & Providencia 2004). Also, the strange mesons ϕ and σ^*, which are often disregarded, are important for the description of hyperon–hyperon interaction, and hence have an important impact on the description of neutrons stars.

The model presented in this paper is constrained by finding the parametrization that best describes symmetric nuclear matter properties (effective nucleon mass and the compressibility modulus at saturation density) and asymmetric matter properties (symmetry energy and its slope), for fixed values of saturation density and binding energy. We determine the hyperon–meson coupling constants for the vector mesons by the SU(6) symmetry relations and the scalar meson coupling by the fitting of hyperon potentials to experimental data. We analyze how nuclear matter properties, hyperon–nucleon, and hyperon–hyperon interactions affect the predictions of the neutron star properties. Also, we identify the effects of the new mesonic degrees of freedom on these properties.

The paper is organized as follows. In Section 2 we present the many-body formalism introduced in the Lagrangian density and analyze its effects on the EOS and chemical equilibrium for the model; the nuclear matter properties at saturation density are calculated in Section 3, when we set the parameters of the model; Section 4 is dedicated to the study of asymmetric matter; we discuss the astrophysical applications of the model in the description of hyperon stars concerning the meson fields and hyperon interactions in Section 5 and, finally, we present our conclusions in Section 6.

2. MANY-BODY COUPLING RELATIVISTIC FIELD FORMALISM

2.1. Formalism

As a conventional way of classifying and organizing interaction terms in effective field theory approaches, as well as to introduce a guideline for the strengths of the various couplings, we adopt the concept of naturalness. Naturalness is related to effective interactions field theories that can be truncated within a phenomenological domain of the theory. However, there is no general proof of naturalness property as, although the attempts of lattice QCD and chiral effective fields theories, currently no derivation of the strong interaction lagrangian density is well established. Nevertheless, the validity of naturalness is supported by phenomenology (see, e.g., Vasconcellos et al. 2014).

The formalism developed in Taurines et al. (2001) takes into account many-body contributions to the nuclear force by introducing the concept of naturalness and a parameterized derivative coupling for the mesons. In this extended version of the formalism, we introduce the new mesonic degrees of freedom δ, σ^*, and ϕ. The δ meson is introduced in order to better describe the properties of asymmetric matter, while the strange mesons (σ^*, ϕ) have important impact on hyperon interactions. The general Lagrangian density of the model is:

Table 1
Baryon and Lepton Properties

Particle	Mass (MeV)	I^3	q_b	q_e	s
p	939.6	1/2	1	+1	0
n	938.3	−1/2	1	0	0
Λ	1116	0	1	0	−1
Σ^+	1189	+1	1	+1	−1
Σ^0	1193	0	1	0	−1
Σ^-	1197	−1	1	−1	−1
Ξ^0	1315	+1/2	1	0	−2
Ξ^-	1321	−1/2	1	−1	−2
e^-	0.511	0	0	−1	0
μ^-	105.7	0	0	−1	0

Note. The rows indicate different particles and I^3, q_b, q_e, and s stand for the isopin projection in the z-direction, baryon charge, electric charge, and strangeness, respectively.

$$\begin{aligned}\mathcal{L} = &\sum_b \overline{\psi}_b\Big[\gamma_\mu\Big(i\partial^\mu - g^*_{\omega b\xi}\omega^\mu - g^*_{\phi b\kappa}\phi^\mu - g^*_{\varrho b\eta}I_{3b}\varrho_3^\mu\Big) \\ &- \Big(m_b - g^*_{\sigma b}\sigma - g^*_{\sigma^* b}\sigma^* - g^*_{\delta b}I_{3b}\delta_3\Big)\Big]\psi_b \\ &+ \frac{1}{2}\Big(\partial_\mu\sigma\partial^\mu\sigma - m_\sigma^2\sigma^2\Big) \\ &+ \frac{1}{2}\Big(\partial_\mu\sigma^*\partial^\mu\sigma^* - m_{\sigma^*}^2\sigma^{*2}\Big) + \frac{1}{2}\Big(\partial_\mu\delta_3\partial^\mu\delta_3 - m_\delta^2\delta_3^2\Big) \\ &+ \frac{1}{2}\Big(-\frac{1}{2}\omega_{\mu\nu}\omega^{\mu\nu} + m_\omega^2\omega_\mu\omega^\mu\Big) \\ &+ \frac{1}{2}\Big(-\frac{1}{2}\phi_{\mu\nu}\phi^{\mu\nu} + m_\phi^2\phi_\mu\phi^\mu\Big) \\ &+ \frac{1}{2}\Big(-\frac{1}{2}\varrho^3_{\mu\nu}\varrho_3^{\mu\nu} + m_\varrho^2\varrho^3_\mu.\ \varrho_3^\mu\Big) \\ &+ \sum_l \overline{\psi}_l\gamma_\mu\big(i\partial^\mu - m_l\big)\psi_l. \end{aligned} \tag{1}$$

The subscripts b and l label, respectively, the baryon octet (n, p, Λ^0, Σ^-, Σ^0, Σ^+, Ξ^-, Ξ^0) and lepton (e^-, μ^-) degrees of freedom. The first and last terms represent the Dirac Lagrangian density for baryons and leptons, respectively. The other terms represent the Lagrangian densities of the mesons, where we assume a Klein–Gordon Lagrangian density for the scalar σ, δ, and σ^* fields and a Proca Lagrangian density for the vector ω, ϱ, and ϕ fields. The meson–baryon coupling is introduced by the coupling constants present in the first term of Equation (1). We allow the system to be isospin asymmetric by choosing the z-axis as the axis of isospin quantization and coupling the components δ_3 and ϱ_3 of the isovector fields to the isospin current $\boldsymbol{I}^\mu = \overline{\psi_b}\gamma^\mu I_{3b}\psi_b$, where I_{3b} is the baryon isospin component in the z—direction (see Table 1). In particular, the baryonic scalar ($\rho_{sb} = \overline{\psi_b}\psi_b$) and vector densities ($\rho_b = \psi_b^\dagger\psi_b$) read:

$$\rho_{sb_i} = \frac{1}{2\pi^2}\Bigg[m^*_{b_i}\,k_{F_{bi}}\sqrt{k^2_{F_{bi}} + \left(m^*_{b_i}\right)^2} - \left(m^*_{b_i}\right)^3\ \ln \times\left(\frac{k_{F_{bi}} + \sqrt{k^2_{F_{bi}} + \left(m^*_{b_i}\right)^2}}{m^*_{b_i}}\right)\Bigg], \qquad \rho_{b_i} = \frac{k^3_{F_{bi}}}{3\pi^2}, \tag{2}$$

Table 2
Meson Fields Properties Considered in the Formalism

Meson	Particle	Classification	Coupling constant	Mass (MeV)
σ	σ	Scalar–isoscalar	g_{σ_b}	550
$\boldsymbol{\delta}$	a_0	Scalar–isovector	g_{δ_b}	980
ω_μ	ω	Vector–isoscalar	g_{ω_b}	782
$\boldsymbol{\varrho}_\mu$	ρ	Vector–isovector	g_{ϱ_b}	770
σ^*	f_0	Scalar–isoscalar	$g_{\sigma^*_b}$	975
ϕ_μ	$\boldsymbol{\phi}$	Vector–isoscalar	g_{ϕ_b}	1020

where $k_{F_{bi}}$ and $m^*_{b_i}$ stand for the Fermi momenta and effective masses of each baryon. The baryon, lepton, and meson properties are found in Tables 1 and 2.

The general definition of the meson–baryon couplings are:

$$\begin{aligned} g^*_{\sigma b\zeta} &\equiv m^\star_{\zeta b_i}g_{\sigma b}, \quad g^*_{\delta b\zeta} \equiv m^\star_{\zeta b_i}g_{\delta b}, \\ g^*_{\sigma^* b\zeta} &\equiv m^\star_{\zeta b_i}g_{\sigma^* b}, \quad g^*_{\omega b\xi} \equiv m^\star_{\xi b_i}g_{\omega b}, \\ g^*_{\varrho b\kappa} &\equiv m^\star_{\kappa b_i}g_{\varrho b}, \quad g^*_{\phi b\eta} \equiv m^\star_{\eta b_i}g_{\phi b}, \end{aligned} \tag{3}$$

where the parametric coefficient $m^\star_{\lambda b_i}$ introduces the nonlinear contributions:

$$m^\star_{\lambda b_i} \equiv \left(1 + \frac{g_{\sigma b}\sigma + g_{\sigma^* b}\sigma^* + g_{\delta b}I_{3b}\delta_3}{\lambda\, m_{b_i}}\right)^{-\lambda}, \tag{4}$$

for $\lambda = \xi,\kappa,\eta,\zeta$.

The main motivation for this formalism is to introduce a parameterized derivative coupling that can be expanded in a series of nonlinear couplings terms between the scalar σ, σ^*, and δ mesons. Each term of the expansion correponds to a medium effect contribution from many-body forces. Ultimately, the complete series expansion, controlled by the $\lambda = \xi$, κ,η,ζ parameter, allows the description of genuine many-body forces, which are introduced as medium effects in the mean field approximation.

Each set of parameters generates different EOSs and population profiles and must be analyzed to cover the range of uncertainties of nuclear saturation properties. We emphasize that, since the meson fields change their values with density, the scalar mesons coupling constants present a density dependence through the coupling of the fields. Note, however, that such an approach is thermodynamically consistent.

As a first approach, we consider the so-called *scalar version* of the model, in which the nonlinear contributions affect only the scalar mesons, i.e., $\xi = 0,\kappa = 0,\eta = 0,\zeta \neq 0$. See Vasconcellos et al. (2014) for a discussion of other possible parameterization choices.

The effective mass of baryons in this model reads:

$$m^*_{b_i\zeta} \equiv\ m_{b_i} - m^\star_{\zeta b_i}\Big(g_{\sigma b}\sigma + g_{\sigma^* b}\sigma^* + g_{\delta b}I_{3b}\delta_3\Big), \tag{5}$$

where one can see the influence of the nonlinear contributions of scalar mesons, controlled through the parameter ζ. Furthermore, as the effective mass of baryons depends on the ζ-parameter, the chemical potential of the interacting particles

is also affected by many-body forces as

$$\mu_{b_i}^{*} = \sqrt{k_{f_{b_i}}^2 + \left(m_{b_i}^{*}\zeta\right)^2} + g_{\omega b}\omega + g_{\varrho b} I_{3b}\varrho_3 + g_{\phi b}\phi, \quad (6)$$

where $k_{f_{b_i}}$ is the baryon Fermi momentum and I_{3b} is the baryon isospin projection in the z-direction.

In order to obtain the equations of motion, we perform mean field approximation so that the fields transform as: $\sigma \rightarrow \langle\sigma\rangle = \sigma_0$, $\sigma^* \rightarrow \langle\sigma^*\rangle = \sigma_0^*$, $\omega^\mu \rightarrow \langle\omega^\mu\rangle = \epsilon_0^\mu \omega_0$, $\phi^\mu \rightarrow \langle\phi^\mu\rangle = \epsilon_0^\mu \phi_0$, $\boldsymbol{\varrho}_3^{\boldsymbol{\mu}} \rightarrow \langle\boldsymbol{\varrho}_3^{\boldsymbol{\mu}}\rangle = \epsilon_0^\mu \varrho_{03}$, $\boldsymbol{\delta}_3 \rightarrow \langle\boldsymbol{\delta}_3\rangle = \delta_{03}$, where ϵ_0^μ corresponds to the Kronecker delta and σ_0, ω_0, ϱ_0, δ_0, ϕ_0, and σ_0^* denote the classical expectation values of the meson fields. We then obtain the mean field equations:

$$\begin{aligned}
\sigma_0 &= \frac{1}{m_\sigma^2}\sum_{b_i}\left[g_{\sigma b}\left(m_{\zeta b_i}^{\star}\right) - \frac{g_{\sigma b}}{m_{b_i}}\left(m_{\zeta b_i}^{\star}\right)^{\frac{\zeta+1}{\zeta}} \times \left(g_{\sigma b}\sigma_0 + g_{\delta b}\delta_0^3\, I^{3b} + g_{\sigma_0^* b}\sigma_0^*\right)\right]\rho_{sb_i},\\
\delta_0^3 &= \frac{1}{m_\delta^2}\sum_{b_i}\left[g_{\delta b}\left(m_{\zeta b_i}^{\star}\right) - \frac{g_{\delta b}}{m_{b_i}}\left(m_{\zeta b_i}^{\star}\right)^{\frac{\zeta+1}{\zeta}} \times \left(g_{\sigma b}\sigma_0 + g_{\delta b}\delta_0^3\, I^{3b} + g_{\sigma^* b}\sigma_0^*\right)\right] I^{3b}\,\rho_{sb_i},\\
\sigma_0^* &= \frac{1}{m_{\sigma^*}^2}\sum_{b_i}\left[g_{\sigma^* b}\left(m_{\zeta b_i}^{\star}\right) - \frac{g_{\sigma^* b}}{m_{b_i}}\left(m_{\zeta b_i}^{\star}\right)^{\frac{\zeta+1}{\zeta}} \times \left(g_{\sigma b}\sigma_0 + g_{\delta b}\delta_0^3\, I^{3b} + g_{\sigma^* b}\sigma_0^*\right)\right]\rho_{sb_i},\\
\omega_0 &= \frac{1}{m_\omega^2}\sum_{b_i} g_{\omega b}\rho_{b_i}, \qquad \varrho_0^3 = \frac{1}{m_\varrho^2}\sum_{b_i} g_{\varrho b}\, I^{3b}\,\rho_{b_i},\\
\phi_0 &= \frac{1}{m_\phi^2}\sum_{b_i} g_{\phi b}\rho_{b_i}.
\end{aligned} \quad (7)$$

As the density increases, it is more energetically favorable for the system to populate new degrees of freedom in order to lower its Fermi energy. In particular, due to strong interaction processes, hyperon species are predicted to start to become important at densities around $2\rho_0$, where ρ_0 is the nuclear saturation density. Assuming that the matter is in β-equilibrium, one can easily verify that the many-body forces also play a role in the particle threshold, as each particle species is populated beyond the following threshold:

$$\mu_b^{*} = q_{b_i}\mu_n^{*} - q_{e_i}\mu_e^{*} - g_{\omega b}\omega_0 - g_{\varrho b} I_{3b}\varrho_{03} - g_{\phi b}\phi_0 \geqslant m_{\zeta b_i}^{*}, \quad (8)$$

where q_{b_i} and q_{e_i} represent the baryon and electric charges, respectively, and μ_n^* and μ_e^* are the neutron and electron effective chemical potentials, respectively.

Assuming chemical equilibrium and, depending on the system to be analyzed, isospin symmetry, or charge neutrality, we calculate the EOS for the model from the components of the stress-energy tensor. The pressure and energy density of the model have the standard expressions

$$\begin{aligned}
p = &-\frac{1}{2}m_\sigma^2\sigma_0^2 - \frac{1}{2}m_\delta^2\delta_3^2 - \frac{1}{2}m_\sigma^2\sigma_0^{*^2} + \frac{1}{2}m_\omega^2\omega_0^2 + \frac{1}{2}m_\varrho^2\varrho_{03}^2 + \frac{1}{2}m_\phi^2\phi_0^2\\
&+ \sum_{b_i,l_i}\frac{1}{\pi^2}\left[\left(\frac{k_{f_{b_i,l_i}}^2}{12} - \frac{\left(m_{b_i,l_i}^{*}\right)^2}{8}\right) \times k_{f_{b_i,l_i}}\sqrt{k_{f_{b_i,l_i}}^2 + \left(m_{b_i,l_i}^{*}\right)^2}\right.\\
&\left. + \frac{\left(m_{b_i,l_i}^{*}\right)^4}{8}\ln\left(\frac{k_{f_{b_i,l_i}} + \sqrt{k_{f_{b_i,l_i}}^2 + \left(m_{b_i,l_i}^{*}\right)^2}}{m_{b_i,l_i}^{*}}\right)\right]\\
\varepsilon = &\frac{1}{2}m_\sigma^2\sigma_0^2 + \frac{1}{2}m_\delta^2\delta_3^2 + \frac{1}{2}m_\sigma^2\sigma_0^{*^2} + \frac{1}{2}m_\omega^2\omega_0^2 + \frac{1}{2}m_\varrho^2\varrho_{03}^2 + \frac{1}{2}m_\phi^2\phi_0^2\\
&+ \sum_{b_i,l_i}\frac{1}{\pi^2}\left[\left(\frac{k_{f_{b_i,l_i}}^2}{4} + \frac{\left(m_{b_i,l_i}^{*}\right)^2}{8}\right)k_{f_{b_i,l_i}} \times \sqrt{k_{f_{b_i,l_i}}^2 + \left(m_{b_i,l_i}^{*}\right)^2}\right.\\
&\left. - \frac{\left(m_{b_i,l_i}^{*}\right)^4}{8}\ln\left(\frac{k_{f_{b_i,l_i}} + \sqrt{k_{f_{b_i,l_i}}^2 + \left(m_{b_i,l_i}^{*}\right)^2}}{m_{b_i,l_i}^{*}}\right)\right],
\end{aligned} \quad (9)$$

m_{b_i,l_i}^* stands for $m_{b_i}^*$ for baryons and m_{l_i} for leptons. The many-body contributions are introduced in the effective masses of the baryons and in the scalar mesons, as well as in their coupling constants.

Note that the inclusion of additional meson fields in the model has a direct effect on the behavior of matter at high densities. The presence of the δ meson also affects asymmetric nuclear matter at saturation density. In the following sections, we analyze the results of the formalism proposed in this work for describing the properties of nuclear matter in both low and high densities regimes. In order to study matter at high densities, we discuss the nucleon–hyperon interaction in what follows.

2.2. Nucleon–Hyperon Interaction

Since hyperons are not present in nuclear matter at saturation density and experimental data concerning their interaction are scarce in the literature, many authors in the past proposed models to describe the meson–hyperon coupling (Moszkowski 1974; Glendenning & Moszkowski 1991; Pal et al. 1999). However, in the last decades various efforts were made in order to understand this sector of strong interactions in more detail and, as a consequence, we have some experimental constraints regarding mainly the hyperon–nucleon interaction.

In particular, the existence of bound Λ-hypernuclear states indicates an attractive potential $U_\Lambda^N = -30$ MeV at saturation (Millener et al. 1988). Concerning Σ-nucleon interactions, the

absence of bound states in a survey for Σ atoms (Mares et al. 1995; Bart et al. 1999) and also scattering studies point toward a repulsive potential (for a review of the topic see Friedman & Gal 2007 and references therein). Investigations on quasi-free production of Ξ's indicate an attractive potential of about $U_{\Xi}^{N} = -18$ MeV (Fukuda et al. 1998; Khaustov et al. 2000; Schaffner-Bielich & Gal 2000; for this topic one can check again Friedman & Gal 2007). On the other hand, still little is known about the hyperon–hyperon interaction resulting from the limited knowledge of double-Λ hypernuclei (Gal 2005; Ahn et al. 2013). The few experimental data point toward a weakly attractive U_{Λ}^{Λ} potential (Takahashi et al. 2001; Gal & Millener 2012; Ahn et al. 2013). Nothing can be said about $\Lambda\Xi$ and $\Xi\Xi$ interactions.

In this work, we define the hyperonic coupling constants $g_{\omega Y}$, $g_{\varrho Y}$, $g_{\delta Y}$, and $g_{\phi Y}$ by using the SU(6) spin-flavor symmetry (Dover & Gal 1985; Schaffner et al. 1994) for the vector mesons, described as follows:

$$\begin{aligned} \frac{1}{3}g_{\omega N} = \frac{1}{2}g_{\omega\Lambda} = \frac{1}{2}g_{\omega\Sigma} = g_{\omega\Xi}, \\ g_{\varrho N} = \frac{1}{2}g_{\varrho\Sigma} = g_{\varrho\Xi}, \quad g_{\varrho\Lambda} = 0, \\ -\frac{2\sqrt{2}}{3}g_{\omega N} = 2g_{\phi\Lambda} = 2g_{\phi\Sigma} = g_{\phi\Xi}, \end{aligned} \tag{10}$$

where $N = n, p$, and assuming simple isospin scaling for the coupling of the δ meson:

$$g_{\delta N} = \frac{1}{2}g_{\delta\Sigma} = g_{\delta\Xi}, \quad g_{\delta\Lambda} = 0. \tag{11}$$

Thus, the hyperonic couplings to the vector mesons are proportional to the number of strange quarks present inside each particle. The rule for the isovector mesons is given by the proportion between the nucleon and the hyperon isospin. For example, since the Λ-hyperon is a singlet, it has zero isospin and, therefore, does not couple to the ϱ and δ mesons.

We obtain the hyperon–sigma coupling associated to the attractive interaction between hyperons and nucleons by fitting the potential depths of the hyperons in nuclear matter (Glendenning & Moszkowski 1991; Schaffner et al. 1992):

$$U_{Y}^{N} = g_{\omega Y}\omega_0(\rho_0) - g_{\sigma Y}\sigma_0(\rho_0), \tag{12}$$

following the values of (Schaffner-Bielich & Gal 2000): $U_{\Lambda}^{N} = -28$ MeV, $U_{\Sigma}^{N} = +30$ MeV, and $U_{\Xi}^{N} = -18$ MeV.

At first, we only consider the scalar-$\sigma\omega\varrho\delta\phi$ version of the model, for fixed values of the hyperon potentials. Then, in Section 5, we come back to the role of the σ^*-meson introducing the $\sigma\omega\varrho\delta\phi\sigma^*$ version of the model in order to verify the effects of coupling constants on the macroscopic properties of neutron stars. In particular, we study the effects of the potential depths and of $g_{\sigma^* Y}$ on the maximum mass, radii, and particle abundances of neutron stars.

3. NUCLEAR MATTER PROPERTIES AT SATURATION

Our model should be in agreement with experimental data for the properties of saturated nuclear matter. For this reason, we impose a saturation density of $\rho_0 = 0.15$ fm^{-3}, a binding energy per baryon of $B/A = -15.75$ MeV (Serot & Walecka 1986), and infer the nucleon–meson coupling constants by fitting the standard values of nuclear matter properties at saturation (details in the following). The ζ parameter, associated with the many-body forces, is constrained to describe a realistic (Dirac) effective mass of the nucleon m_N^* at saturation between 0.66 and 0.78 m_N (Johnson et al. 1987; Jaminon & Mahaux 1989), a compressibility modulus K_0 between about 200 and 300 MeV (see Stone et al. 2014, and references therein), a symmetry energy $a_{\rm sym}^0$ between 25 and 35 MeV (Tsang et al. 2012; Lattimer & Lim 2013; Horowitz et al. 2014), and a symmetry energy slope L_0 between 60 and 115 MeV (Chen et al. 2005b; Lopes & Menezes 2014a).

At saturation, the isopin-symmetric nuclear matter has vanishing pressure, and is not populated by leptons nor hyperons (by definition). Also, due to the isospin symmetry, the mean values of the isovector mesons ϱ and δ are zero. To determine the constants $(g_{\sigma N}/m_\sigma)^2$, $(g_{\omega N}/m_\omega)^2$, and the effective mass of the nucleon m_N^* at saturation, we solve the system of equations of zero pressure, experimental value of the binding energy per nucleon and the σ_0 field equation of motion self-consistently.

We calculate the compressibility modulus for symmetric nuclear matter, which is related to the curvature of the EOS by:

$$K_0 = 9\rho_0\left[\frac{d(\varepsilon/\rho)}{d\rho}\right]_{\rho=\rho_0}, \tag{13}$$

where K_0 corresponds to the value of the compressibility modulus at saturation density ρ_0 and ϵ is the corresponding energy density of the system. It is important to note that the ζ-parameter relates the effective mass to the compressibility modulus (Dexheimer et al. 2008), meaning that for each choice of ζ, K_0 is calculated independently and is not used as an input to parameterize the model, as is the case in most RMF models.

The values of $(g_{\sigma N}/m_\sigma)^2$, $(g_{\omega N}/m_\omega)^2$, m_N^*, and K_0 for different choices of parametrizations (different ζ) are shown in Table 3. Figure 1 shows that these quantities rapidly converge as a function of ζ, leaving a small range of values of m_N^* and K_0 that fit the experimental values. We remark that low values of the parameter ζ (lower effective mass and higher compressibility modulus) generate stronger coupling constants for the scalar σ-meson as well as for the vector ω-meson. The decrease of the attraction provided by the many-body forces (through the scalar mesons) together with the constant coupling of the vector mesons allows matter to be more repulsive for smaller values of the ζ parameter. We also checked the dependence of the binding energy as a function of density on the many-body forces parameter, from which we have found that larger values of the ζ parameter allow for more bound, i.e., more attractive matter. This behavior of matter has a direct impact on the EOS for higher densities and, thus, on the observational properties of neutron stars, as we discuss in Section 5.

In order to determine the coupling constants of the nucleon with respect to the isovector mesons, we must fit the properties of asymmetric nuclear matter. When only the ϱ meson is considered, the respective coupling constant is fitted to the symmetry energy and the value of the slope of the symmetry energy at saturation is obtained directly from that. However, as pointed out by Lopes et. al. (Lopes & Menezes 2014a), the inclusion of the δ meson breaks this relation. In this case, it is necessary to consider the EOS of asymmetric nuclear matter (in

Table 3
Normalized Effective Mass of the Nucleon, Compressibility Modulus, and Coupling Constants for Different Parametrizations of the Model (Different ζ's)

ζ	m_n^*/m_n	K_0 (MeV)	$(g_{\sigma N}/m_\sigma)^2$	$(g_{\omega N}/m_\omega)^2$
0.040	0.66	297	14.51	8.74
0.045	0.67	282	14.22	8.40
0.049	0.68	272	13.99	8.14
0.054	0.69	262	13.71	7.83
0.059	0.70	253	13.44	7.55
0.065	0.71	244	13.12	7.23
0.071	0.72	237	12.82	6.94
0.078	0.73	230	12.50	6.63
0.085	0.74	225	12.21	6.37
0.094	0.75	220	11.86	6.05
0.104	0.76	216	11.53	5.75
0.115	0.77	213	11.20	5.46
0.129	0.78	211	10.84	5.16

the absence of leptons) and solve the system of equations of the symmetry energy and its slope to find the corresponding values of $(g_{\varrho N}/m_\varrho)^2$ and $(g_{\delta N}/m_\delta)^2$, according to

$$a_{\rm sym}^0 = \frac{1}{2}\left[\frac{d^2(\varepsilon/\rho)}{dt^2}\right]_{t=0}, \quad L_0 = 3\rho_0\left[\frac{da_{\rm sym}}{d\rho}\right]_{\rho=\rho_0}, \qquad (14)$$

where the asymmetry between protons and neutrons is quantified by $t = (\rho_p - \rho_n)/\rho_b$.

It is important to note that, in this formalism, the many-body contributions correlate the effective mass of the nucleon and the scalar field equations in the presence of the delta meson (see Equation (4)). In other words, to determine the EOS of asymmetric matter at saturation, it is necessary to first solve self-consistently a system of equations for the expressions of $m_N^*(m_N^*, \sigma_0, \delta_0)$, $\sigma_0(m_N^*, \sigma_0, \delta_0)$ and $\delta_0(m_N^*, \sigma_0, \delta_0)$ for a non-vanishing isospin system.

The slope of the symmetry energy has become a very prominent constraint for the EOS in the past years, as its measurements (through, for example, neutron skin experiments) have become more accurate. These results seem to indicate low values ($L_0 \lesssim 60$ MeV) for this quantity (Steiner & Gandolfi 2012; Lattimer & Lim 2013; Li & Han 2013). Note, however, that some works (such as those in Chen et al. 2005b; Tsang et al. 2012; Cozma et al. 2013; Wang et al. 2014 and Sotani et al. 2015) found much higher values for the slope of the symmetry energy $L_0 \gtrsim 90$ MeV. Because its values still lie in a large accepted range, we perform a large scan of values with our model in order to find the isovector-mesons coupling constants suitable to describe massive hyperon stars.

In summary, the methodology used to describe nuclear properties in this formalism is the following: by the analysis of the properties of symmetric matter at saturation, we choose the nonlinearity parameter ζ that will determine the $g_{\sigma N}$ and $g_{\omega N}$ coupling constants and give the values of the effective mass of the nucleon and the compressibility modulus by a one-to-one relation. However, since the choice of the parameter ζ is not enough to determine $g_{\varrho N}$ and $g_{\delta N}$ uniquely, we must analyze the new parameter space given by the isovector meson coupling constants, the symmetry energy and its slope as shown in Figures 2–4 for different choices of ζ.

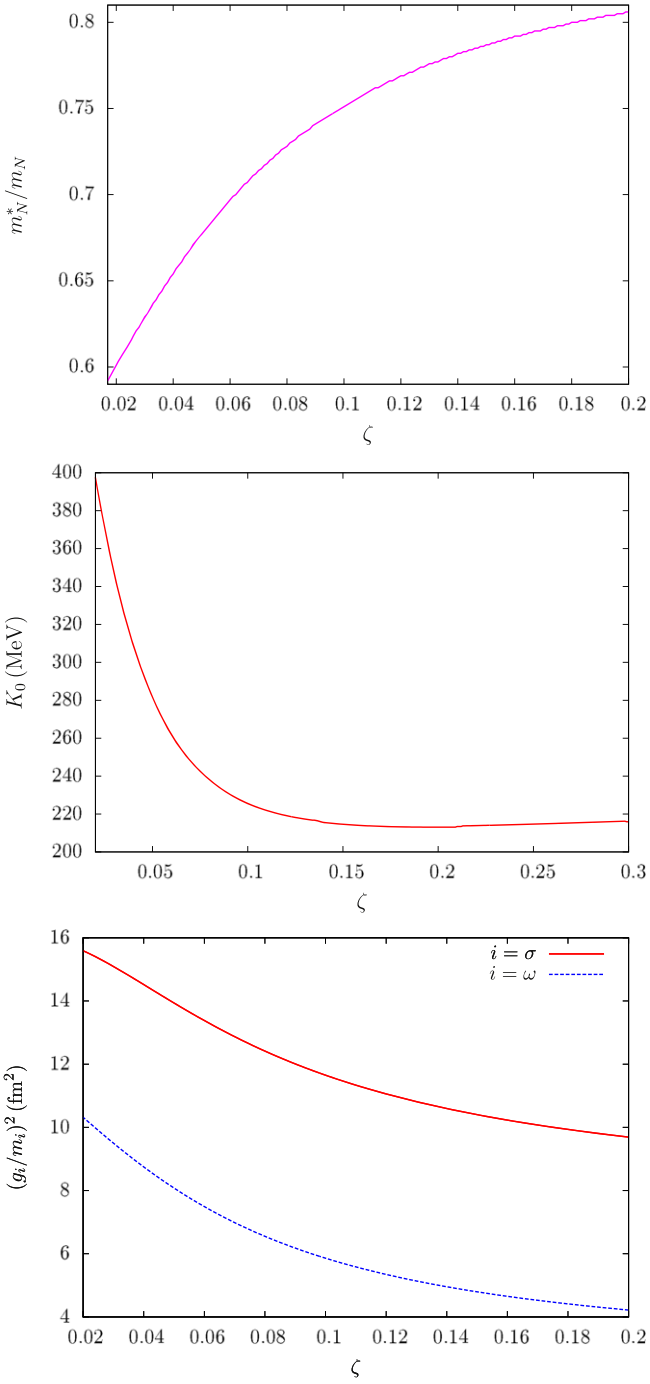

Figure 1. Nuclear matter properties at saturation densitiy as a function of the parameter ζ. The top panel shows the effective mass of the nucleon m_N^*, the middle panel shows the compressibility modulus K_0, and the bottom panel shows the coupling constants of the mesons σ and ω.

Differently from the case of symmetric matter, where for a given value of the effective nucleon mass there is only one possible value for the compressibility modulus Figures 1–4 show that for a given value of the symmetry energy $a_{\rm sym}^0$, one can have different values of the slope L_0. The choices of $a_{\rm sym}^0$ and L_0 result in different values of the coupling constants of the mesons ϱ and δ, and are also dependent on the parameter ζ.

The parameter space for $\zeta = 0.040$ is shown in Figure 2. The panels show the coupling constants in a color scale as a

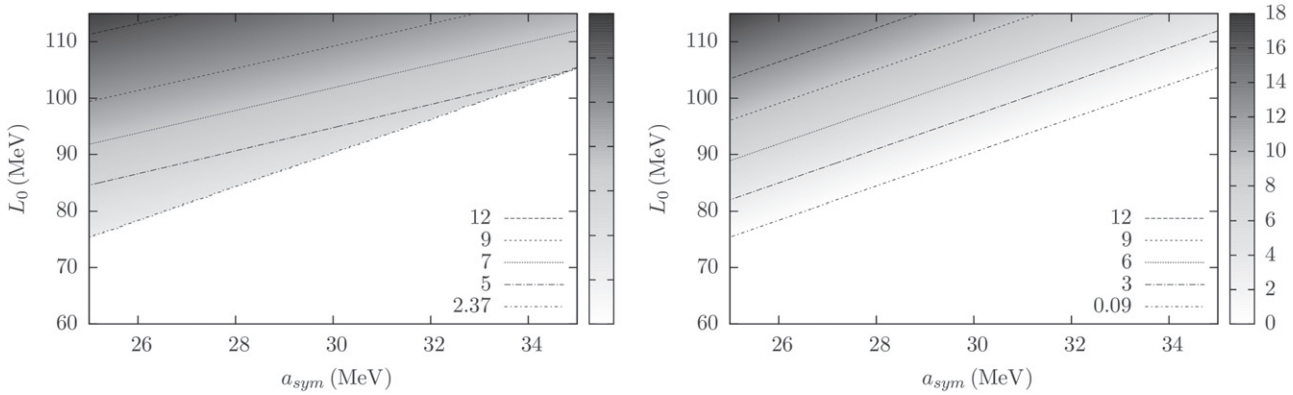

Figure 2. Possible values of $a_{\rm sym}^0$ and L_0 for $(g_{\varrho N}/m_\varrho)^2$ (left panel) and $(g_{\delta N}/m_\delta)^2$ (right panel) for $\zeta = 0.040$. The intensity of each coupling is plotted in a color sequence and also indicated by the different types of lines.

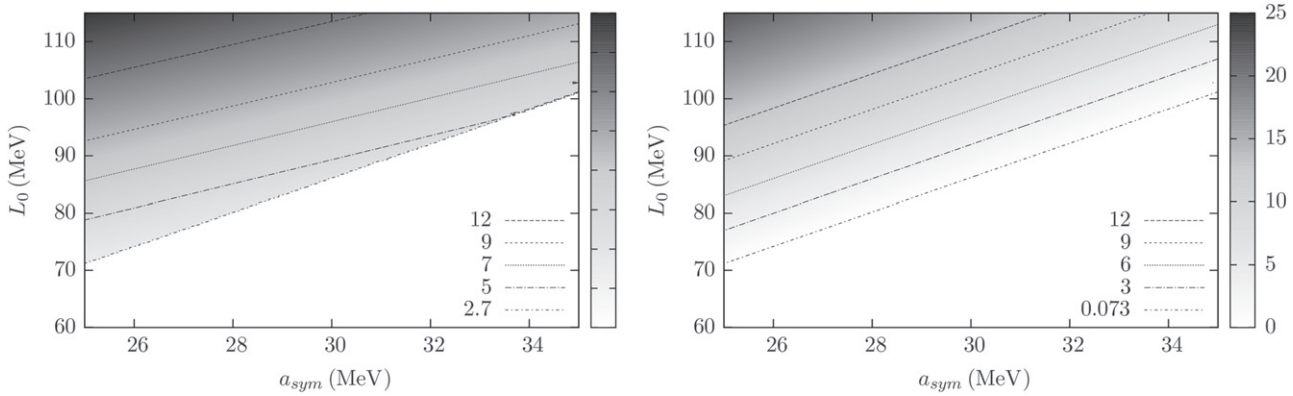

Figure 3. Same as Figure 2 for $\zeta = 0.071$.

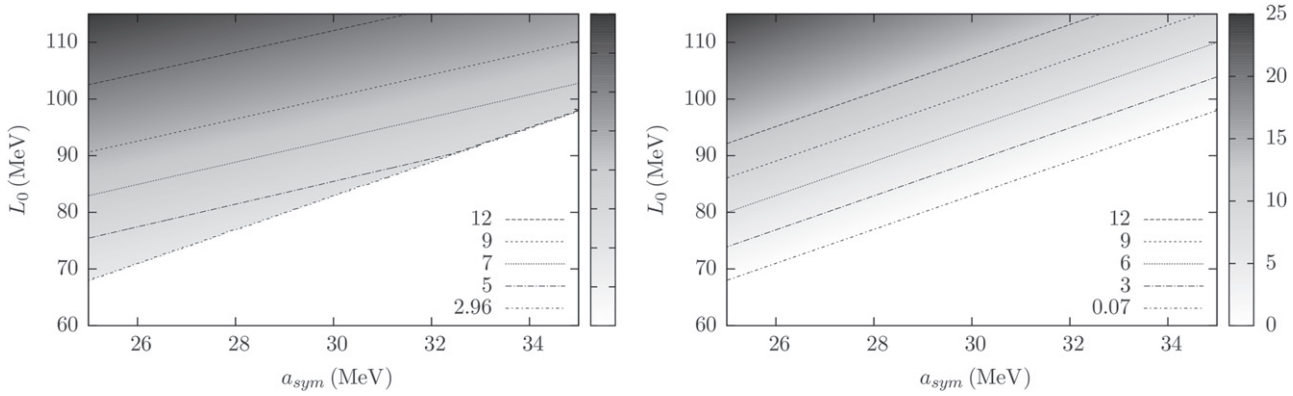

Figure 4. Same as Figure 2 for $\zeta = 0.129$.

function of $a_{\rm sym}^0$ and L_0. The color scale on the left panel corresponds to the values of $(g_{\varrho N}/m_\varrho)^2$. The same is shown for $(g_{\delta N}/m_\delta)^2$ on the right panel. The white regions in the figures correspond to the cases where no numerical solution for the system of equations exists. Obviously, the values of the coupling constants must be selected simultaneously in both panels, in order to guarantee that their values are associated with the same solutions for $a_{\rm sym}^0$ and L_0.

Note that, by the comparison between different choices of the parameter ζ, there is a substantial change in the possible range of solutions for the same values of the coupling constants. For example, comparing the right panels in Figures 2 and 4, one verifies that the solution for $(g_{\delta N}/m_\delta)^2 = 12\text{fm}^2$ is found in the interval of $a_{\rm sym}^0 \simeq 25-27$ MeV and $L_0 \simeq 111-115$ MeV for $\zeta = 0.040$, while for $\zeta = 0.129$ the interval is increased to $a_{\rm sym}^0 \simeq 25-31.5$ MeV and $L_0 \simeq 102-115$ MeV. This analysis was carried out only in the range of $25 \leqslant a_{\rm sym}^0 \leqslant 35$ MeV and $60 \leqslant L_0 \leqslant 115$ MeV in this work.

The maps for the symmetry energy and its slope show that the minimum values found for the asymmetry energy slope are those that correspond to the higher values of the parameter ζ. The lowest value for the slope can be seen in Figure 4, where for $a_{\rm sym}^0 = 25$ MeV, the solution of $L_0 = 68$ MeV is associated with $(g_{\varrho N}/m_\varrho)^2 = 2.96$ fm^2 (left panel) and $(g_{\delta N}/m_\delta)^2$=0.07 fm^2

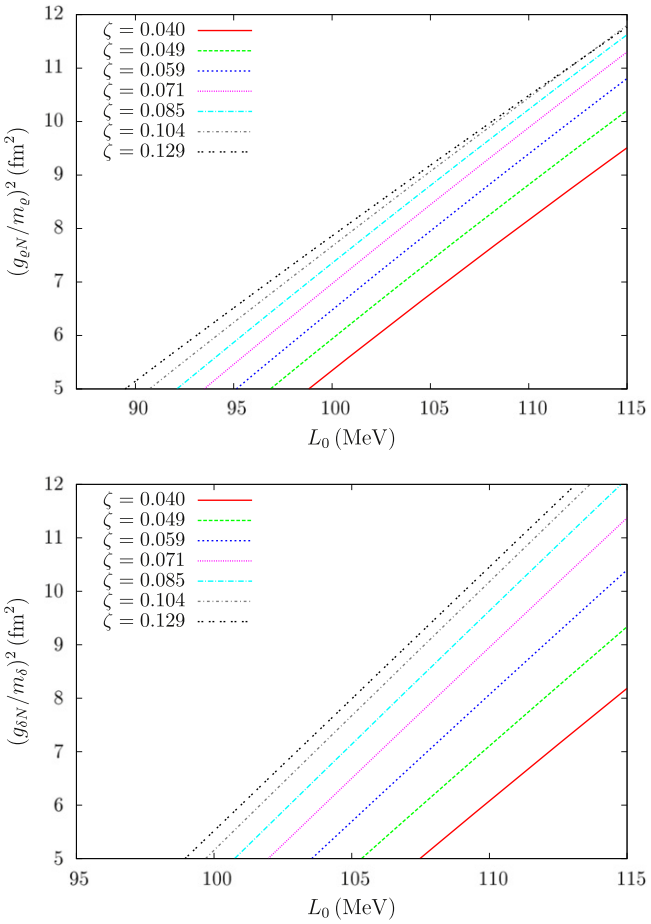

Figure 5. $(g_{\varrho N}/m_\varrho)^2$ (left panel) and $(g_{\delta N}/m_\delta)^2$ (right panel) dependence on the slope of the symmetry energy L_0 for different value of the ζ parameter. The plots correspond to the symmetry energy $a_{\rm sym}^0 = 32$ MeV.

(right panel). Figure 5 allows us to better visualize the relation between the coupling constants intensity and the slope L_0 for different choices of ζ. The left and right panels show simultaneous solutions for $(g_{\varrho N}/m_\varrho)^2$ and $(g_{\delta N}/m_\delta)^2$, from which we verify a linear relation with respect to the slope of the symmetry energy L_0. The higher values of the parameter ζ are those which provide lower L_0 values, but higher coupling constants $(g_{\varrho N}/m_\varrho)^2$ and $(g_{\delta N}/m_\delta)^2$. In particular, this result is important in the light of recent works pointing toward low values of L_0 (Hebeler et al. 2013), meaning that the δ meson contribution should not be too large.

A recent work by Dutra et al. that carries out a review of 263 parametrizations of different RMF models reported that the value of the volume part of the isospin incompressibility, denoted $K_{\tau v}$, can also be used as a constraint for the description of nuclear matter (Dutra et al. 2014). This quantity reads:

$$K_{\tau v}^0 = \left(K_{\rm sym}^0 - 6L_0 - \frac{Q_0}{K_0} L_0 \right), \tag{15}$$

where K_0 and L_0 are the compressibility modulus and the slope of the symmetry energy at saturation. The quantities Q_0 and $K_{\rm sym}^0$ are the skewness coefficient of the EOS and the curvature

Table 4
Volume Part of The Isospin Incompressibility $K_{\tau v}$, Curvature of The Symmetry Energy $K_{\rm sym}^0$, Skewness Coefficient of the Symmetry Energy $Q_{\rm sym}^0$, and of the Equation of State Q_0 at Saturation for Different Parametrizations of the Model

ζ	$K_{\tau v}^0$ (MeV)	$K_{\rm sym}^0$ (MeV)	$Q_{\rm sym}^0$ (MeV)	Q_0 (MeV)
0.040	−558	30.85	184.5	21.3
0.049	−484	31.23	197.8	−188.2
0.059	−412	30.72	192.3	−364.6
0.071	−346	29.30	176.1	−505.9
0.085	−291	27.36	150.4	−612.1
0.104	−243	25.01	114.8	−698.8
0.129	−214	22.57	78.3	−751.1

Note. The values of the symmetry energy and its slope are fixed to $a_{\rm sym}^0 = 32$ MeV and $L_0 = 97$ MeV.

of the symmetry energy, respectively:

$$Q_0 = 27\rho_0^3 \left(\frac{d^3(\varepsilon/\rho)}{d\rho^3} \right)_{\rho=\rho_0, t=0},$$
$$K_{\rm sym}^0 = 9\rho_0^2 \left(\frac{d^2(a_{\rm sym})}{d\rho^2} \right)_{\rho=\rho_0}. \tag{16}$$

The values of $K_{\tau v}^0$ and Q_0 lay in a wide range of uncertainties, $K_{\tau v}^0 = -550 \pm 150$ MeV that come from the overlap of the analysis of isospin diffusion (Chen et al. 2005a), neutron skin (Centelles et al. 2009) and measurement of Sn isotopes (Li et al. 2007), and $Q_0 = -700 \pm 500$ MeV from the investigation of isoscalar giant monopole resonance (Farine et al. 1997; Khan & Margueron 2013; for indirect methods, see Steiner et al. 2010; Chen 2011). We have also calculated the symmetry energy skewness at saturation $Q_{\rm sym}^0 = 27\rho_0^3 (\frac{d^3 a_{\rm sym}}{d\rho^3})_{\rho=\rho_0}$, and the values of all these quantities for different parametrizations of the model are shown in Table 4.

We find that the parametrizations $\zeta = 0.040$–0.071 present values of $K_{\tau v}^0$ in agreement with the literature. The results for the skewneess coefficient Q_0 for the parametrizations $\zeta = 0.040$ and $\zeta = 0.049$, are smaller than the threshold value. However, we must emphasize that the quantities analyzed in Table 4 have a wide range of uncertainties and are based on the overlap of experimental data that carry large uncertainties themselves. Also, the calculation of these quantities depends directly on the values of the symmetry energy and its slope and the results presented in Table 4 are for fixed values of the $a_{\rm sym}^0$ and L_0. A wider study regarding these quantities is out of the scope of this present work.

4. PROPERTIES OF ASYMMETRIC NUCLEAR MATTER AT HIGH DENSITIES

Before turning our attention to neutron star matter, we discuss the behavior of asymmetric matter properties at high densities. The symmetry energy and its slope can be used to extrapolate the description of nuclear matter to isospin asymmetric nuclear matter at higher densities. Also, as was already pointed out by Lopes et al. (Lopes & Menezes 2014a) and other authors, the behavior of the properties of asymmetric nuclear matter in the high density regime has a significant impact on the observable properties of neutron stars.

Allowing matter to be populated by nucleons and hyperons, we assume conserved isospin (e.g., purely neutron matter only or symmetric matter only) and baryon number, and set the strangeness chemical potential μ_s to zero. We start by calculating the compressibility for symmetric nuclear matter as a function of the density, using the general expression

$$K(\rho) = 9\left(\frac{dP}{d\rho}\right)_{t=0}. \quad (17)$$

The behavior of the compressibility as a function of density is shown in the top panel of Figure 6 for different choices of the parameter ζ and for fixed values of the hyperon potentials ($U_\Lambda^N = -28$ MeV, $U_\Sigma^N = 30$ MeV, $U_\Xi^N = -18$ MeV), symmetry energy $a_{\rm sym}^0 = 32$ MeV and slope $L_0 = 97$ MeV at saturation. The results shown in the top panel of Figure 6 point to the fact that the lower values of ζ generate higher values of the compressibility for high densities, analagously to the behavior at saturation density.

The impact of the appearance of new degrees of freedom can be verified at densities around 0.5 and 0.7 fm^{-3}, which correspond to the densities where the Λ and Ξ hyperons appear. As the density increases and new degrees of freedom are populated, the compressibility modulus decreases due to the softening of the EOS (when a hyperon appears). The density continues to increase and the Fermi momentum of the new particle species increases, making the EOS stiff again, until another particle appears.

We calculate the symmetry energy and its slope by extending the expressions in Equation (14) to higher densities. The respective results are shown in middle and bottom panels of Figure 6 and correspond, again, to different choices of the parameter ζ at fixed values of the hyperon potentials, symmetry energy $a_{\rm sym}^0 = 32$ MeV and slope $L_0 = 97$ MeV at saturation. Figure 6 shows that the symmetry energy is not affected by the parameter ζ at low densities, as expected from our previous fitting, and starts to present an interesting behavior only for densities of about $3\rho_0$, which correspond to the point where hyperons (appear for symmetric matter).

For fixed values of $a_{\rm sym}^0$ and its slope L_0 at saturation, higher values of the ζ parameter introduce larger differences between symmetric and asymmetric matter EOS's. This behavior is due to the fact that the coupling constants of the isovector mesons are also dependent on the values of the ζ parameter, generating a competition between the attraction and repulsion from the isoscalar and isovector mesons. In particular, higher values of ζ generate stronger couplings of the ϱ meson, which contribute only to the asymmetric EOS and are of importance at high densities. The strongest repulsive contribution provided by the higher values of the ζ parameter (higher ϱ couplings) allows for a stiffer EOS that differs more from the symmetric EOS (in the absence of the isovector mesons contributions) and, since the symmetry energy relates precisely this difference, the parametrization with higher values of ζ yields higher values of the symmetry energy as a function of density.

Since the symmetry energy and the slope of the symmetry energy are correlated quantities, it is natural that they present a similar behavior: the higher (lower) the ζ parameter, the higher (lower) are the values of the symmetry energy and its slope as a function of the density. The peaks in bottom panel of Figure 6 are again due to the appearance of the hyperons.

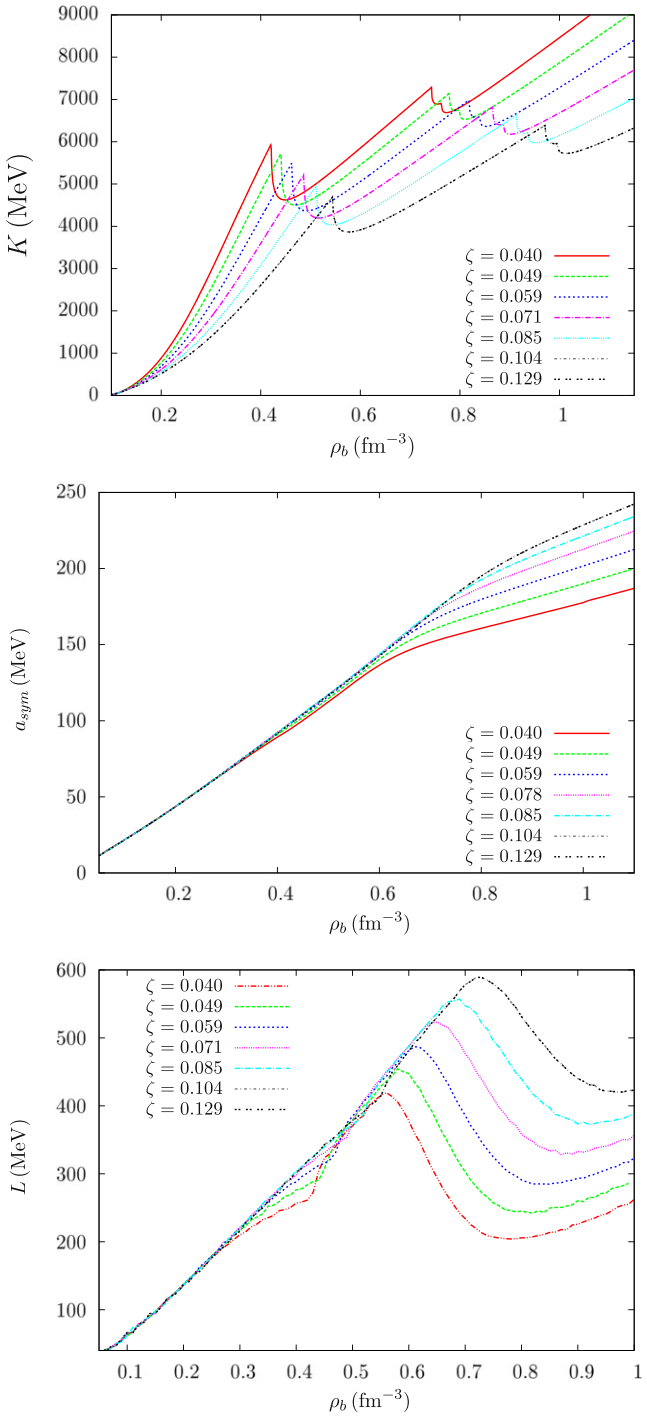

Figure 6. Properties of asymmetric matter (containing hyperons) as a function of baryon density. The compressibility modulus $K(\rho)$ (top panel), symmetry energy $a_{\rm sym}(\rho)$ (middle panel), and slope $L(\rho)$ (bottom panel) are plotted for different choices of ζ.

It is worth mentioning that different values of the symmetry energy $a_{\rm sym}^0$ and its slope L_0 at saturation also have an impact on their behavior at higher densities. In particular, smaller values of $a_{\rm sym}^0$ and higher values of L_0 allow for a higher increase in the slope. We will come back to this topic in next section, when the impact of these properties on the radii of neutron stars is investigated.

Finally, we mention that, although the meson fields are density dependent in every RMF model, in the formalism

adopted in this work the coupling between baryons and scalar mesons depends on the nonlinear contributions of the meson fields themselves. This feature of the model implies that the behavior of the scalar mesons effective coupling constants ($g^*_{\sigma b}$, $g^*_{\delta b}$, and $g^*_{\sigma^* b}$) as a function of the density is affected by the many-body contributions, generating a direct impact on the baryon effective masses and, consequently, on the global behavior of the matter. This behavior is quantified in Figures 7 and 8, where we show the effective coupling constants of the scalar mesons and the effective mass of the nucleons as a function of baryon density. We show results for different versions of the model (with different meson content) as well as different choices of the ζ parameter.

In the top panel of Figure 7, we show that the introduction of the δ meson breaks the isospin degeneracy in the coupling constants of protons and neutrons. The difference is more pronounced for higher values of ζ, which correspond to stronger many-body contributions. The delta meson increases the positive isospin particles coupling with respect to the scalar mesons and decreases the coupling for negative isospin particles, meaning that the first generates more attraction. On the other hand, from Equation (7), one can see that the isospin of the particles affects all scalar mesons non-trivially due to the nonlinear contributions. Hence, the competition between the amount of particles with positive and negative isospin plays an important role for the global attractive or repulsive response of matter.

The introduction of the σ^* meson has impact on all of the scalar field equations as well. The top and middle panels of Figure 7 show that this meson contributes to a faster decrease of the effective coupling constants, due to its extra contribution to the many-body forces that change the couplings. Also, from the bottom panel of Figure 7 one can see that the proton and neutron coupling constants departure from the degenerate case is more notable when all scalar fields, together with higher values of the many-body forces contribution, are assumed.

The effective mass of the nucleon as a function of the density in Figure 8 presents a similar response to the introduction of the δ and σ^* mesons. The δ meson splits the masses of protons and neutrons and the σ^* meson makes their decrease faster due to the extra contribution in the many-body forces. Both effects are extremely relevant to the chemical equilibrium and, consequently, to the global behavior of the matter. In the next section, we will come back to the effects of the σ^* meson for neutron star matter with hyperons.

5. ASTROPHYSICAL APPLICATION

In this section, we apply the formalism developed so far to describe hyperon matter inside neutron stars. We compare our predictions with the recently observed massive neutron stars PSR J038+0432 and PSR J1614-2230 (Demorest et al. 2010; Antoniadis et al. 2013). We have already shown that our model is in agreement with nuclear matter properties at saturation density, and now a comparison with astrophysical properties characterizes a second test of the underlying microscopic model. In addition, aiming to verify the impact of future hypernuclear data in the context of neutron stars, we investigate the effects of different values of the hyperon potentials and the coupling constant of the σ^*-meson on macroscopic properties of neutron stars.

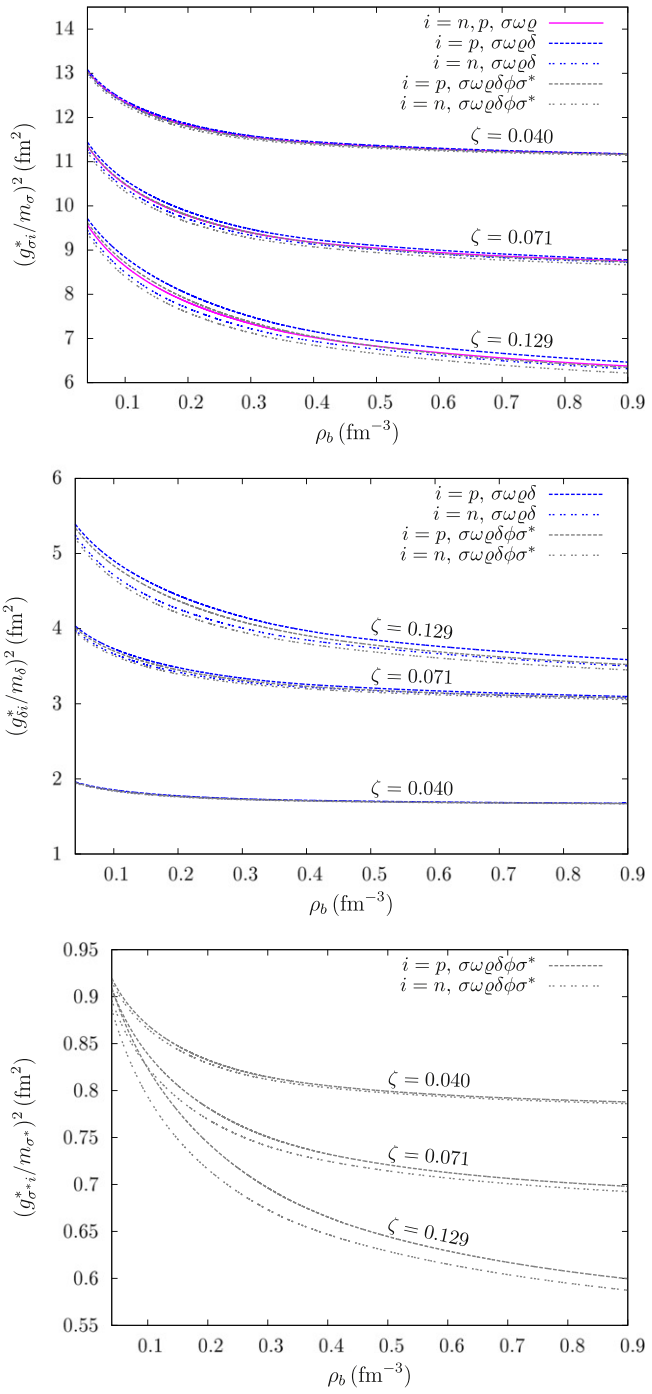

Figure 7. Effective coupling constants of the scalar mesons as a function of baryon density. The coupling of the σ (top panel), δ (middle panel), and σ^* (bottom panel) are plotted for protons and neutrons for different values of ζ. The different versions of the model are indicated by colors: $\sigma\omega\varrho$ (magenta), $\sigma\omega\varrho\delta$ (blue), and $\sigma\omega\varrho\delta\phi\sigma^*$ (gray).

Assuming that matter is in β-equilibrium and is locally charge neutral, we use the EOS of the model as an input to solve the Tolman–Oppenheimer–Volkoff (TOV) equations (Tolman 1939; Oppenheimer & Volkoff 1939) and obtain the macroscopic structure of stars for different parametrizations. The EOS and the mass–radius diagram for each parametrization studied, including hyperons, can be found in Figures 9 and 10, respectively.

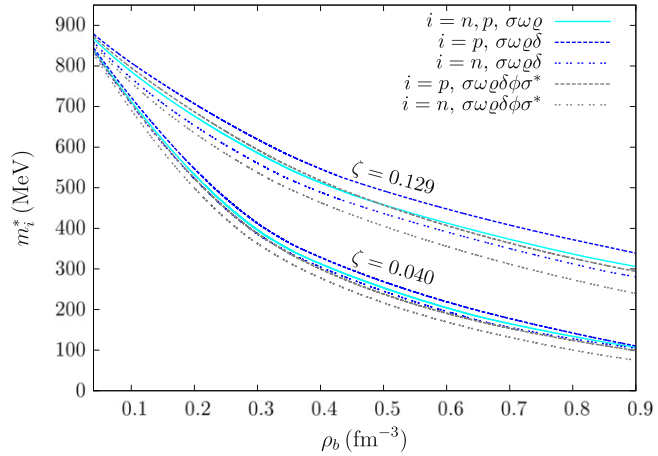

Figure 8. Effective mass of protons and neutrons as a function of baryon density for $\zeta = 0.040$ and $\zeta = 0.129$. Each color corresponds to a different version of the model.

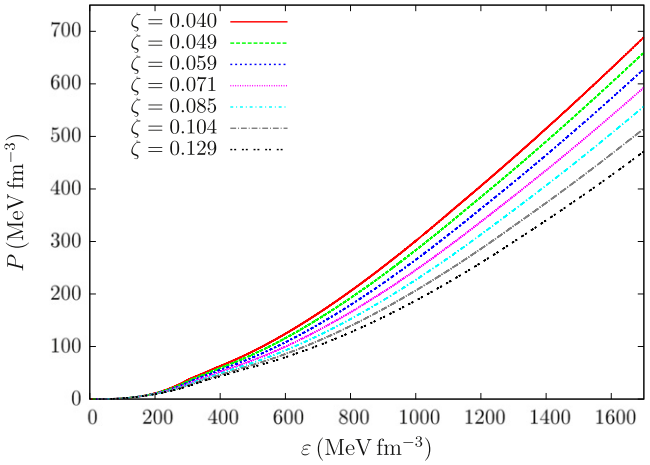

Figure 9. Equation of state for star matter shown for different parameter sets.

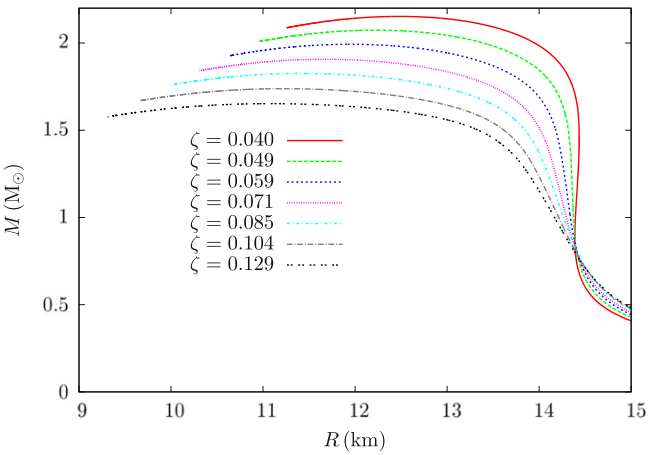

Figure 10. Mass–radius relation for star matter shown for different sets of parameters.

5.1. The Role of ζ on the Properties of Hyperon Star

The dependence of the EOS on the parameters of the model is shown in Figure 9. In particular, the lowest value of ζ generates the stiffer EOS and, consequently, allows for a higher stellar mass. The argument here is the same as the one discussed in Section 3: since a stiffer EOS is related to higher values of the internal pressure of the system and, accordingly, to higher values of the compressibility modulus of nuclear matter, this in turn requires stronger contributions from repulsive components of the nuclear force. In our general approach, however, many-body forces lower the strengths both of attractive and repulsive interaction terms due to *shielding effects*, which result in higher (lower) values of the compressibility modulus of nuclear matter in the case of higher (lower) relative reduction of the attractive contributions. Our present results are consistent with the analysis above, since we have obtained a stiffer EOS for lower values of the ζ parameter, which corresponds to stronger repulsion.

In summary, lower values of the ζ parameter generate more repulsive nuclear matter which is able to support more gravity and, consequently, create a macroscopic object with higher mass. In particular, the highest stellar mass generated by the extended version of model including hyperons is 2.15 $M_\odot$ (for $\zeta = 0.040$), in agreement with pulsars PSR J16142230 ($M = 1.97 \pm 0.04\, M_\odot$) (Demorest et al. 2010), and PSR J0348+0432 ($M = 2.01 \pm 0.04\, M_\odot$) (Antoniadis et al. 2013), as is shown in Figure 10.

For completeness, in Table 5 we present results of different versions of the model. The first and second columns represent different meson content versions of the model and values of the ζ parameter, respectively. We also show maximum mass results for nucleonic and hyperon stars, in the third and fourth columns, respectively. Also, since the $\sigma\omega\varrho$ version of the model has a one-to-one relation between $a_{\rm sym}^0$ and L_0, we show values of L_0 in the fifth column.

All nucleonic stars in the range of parameters of $\zeta = 0.040$–0.129 are in agreement with observational data. In particular, the most massive nucleonic star described by the model is the one for $\zeta = 0.040$, with 2.57 $M_\odot$. We also verify that the inclusion of the δ meson does not affect significantly the maximum mass of the stars, introducing a difference of only 0.01 $M_\odot$ in the model. The weak contribution of the δ meson in the results comes from the low values of $g_{\delta N}$ chosen in order to reproduce low values of the slope L_0.

The δ meson introduces a repulsion between protons and neutrons. As this repulsion favors the neutron population, the Fermi momenta of neutrons harden the EOS, generating more massive nucleonic stars. In the case of hyperon stars, the δ meson shifts the appearance of hyperons to lower densities, preventing a strong stiffening of the EOS and even softening it in some cases. Therefore, in general, for the nucleonic stars, the δ meson has the effect of increasing the maximum star mass, while for hyperon stars, the meson decreases its maximum value (Menezes & Providencia 2004).

Assuming that hyperons are present in compact stars, ensuring that the model is in accordance with the observational data puts additional constraints on nuclear properties at saturation. The comparison between the parametrizations in Tables 3 and 5 shows that the version of the model presented in this work constrains the effective mass of the nucleon and the compressibility modulus on ranges of 0.66–0.70 m_N and 253–297 MeV (associated to the range of $\zeta = 0.040$–0.059), respectively. Also, from the parametrization $\zeta = 0.059$, the lowest values of the slope in agreement with nuclear and observational data is $L_0 = 94$ MeV (for $a_{\rm sym}^0 = 32$ MeV). Such a conclusion can be reached because a change in the slope

Table 5
Maximum Masses of Nucleonic and Hyperon Stars for Different Versions of the Model, L_0, and ζ-Parameter

Model	ζ	$M_{\max}^{\text{nucleonic}}(M_\odot)$	$M_{\max}^{\text{hyperon}}(M_\odot)$	L_0 (MeV)
$\sigma\omega\varrho$	0.040	2.57	1.90	96.16
	0.049	2.49	1.83	94.68
	0.059	2.41	1.76	93.22
	0.071	2.32	1.69	92.05
	0.085	2.24	1.62	90.92
	0.104	2.15	1.55	89.82
	0.129	2.06	1.49	88.86
$\sigma\omega\varrho\delta$	0.040	2.57	1.90	97.0
	0.049	2.50	1.83	97.0
	0.059	2.42	1.76	97.0
	0.071	2.33	1.68	97.0
	0.085	2.25	1.61	97.0
	0.104	2.16	1.55	97.0
	0.129	2.07	1.49	97.0
$\sigma\omega\varrho\delta\phi$	0.040	2.57	2.15	97.0
	0.049	2.50	2.07	97.0
	0.059	2.42	1.99	97.0
	0.071	2.33	1.91	97.0
	0.085	2.25	1.83	97.0
	0.104	2.16	1.74	97.0
	0.129	2.07	1.65	97.0

Note. The hyperon potentials are fixed to $U_\Lambda^N = -28$ MeV, $U_\Sigma^N = +30$ MeV $U_\Xi^N = -18$ MeV and the symmetry $a_{\text{sym}}^0 = 32$ MeV.

L_0 from 97 to 115 MeV only contributes to a tiny decrease of less that 0.0035 $M_\odot$ in the maximum mass of stars. We also find a decrease of 0.01 $M_\odot$ in the maximum star mass when the symmetry energy a_{sym}^0 is changed from 30 to 33 MeV.

One can also clearly see from Figure 10 that the radius of the star is affected by the ζ parameter. We will come back to this topic in Section 5.4, where we investigate all quantities that affect the radius of the canonical star.

In the last section, it was discussed that the many-body contributions present in the scalar meson couplings have a direct influence on the behavior of particles in hyperonic matter, since they affect the chemical equilibrium equations. Also, since the ζ parameter dictates the strength of the nonlinear contributions, we analyze its effects on the particle population in Figure 11. The figure shows the fraction of particles as a function of baryon density for two choices of parameters and for fixed values of the hyperon potentials, symmetry energy $a_{\text{sym}}^0 = 32$ MeV, and slope $L_0 = 97$ MeV at saturation.

The results in Figure 11 show that, as the value of ζ increases, the densitiy corresponding to the appearance of each hyperon is shifted to higher values. For the choices $\zeta = 0.040$ (left panel) and $\zeta = 0.129$ (right panel), the thresholds of the Λ^0, Ξ^- and Ξ^0 hyperons are shifted from 0.30 to 0.36 fm^{-3}, 0.38 to 0.45 fm^{-3}, and 0.90 to 1.1 fm^{-3}, respectively. Although the dependence of the beta equilibrium on the ζ parameter, one can also verify that the threshold for the μ^- lepton is not strongly affected.

In order to specify the strangeness content of the stars, we define the parameter f_s

$$f_s = \sum_i \frac{\rho_i Q_{s_i}}{\rho_b} = \frac{\rho_\Lambda + \rho_\Sigma + 2\rho_\Xi}{\rho_b}, \quad (18)$$

that corresponds simply to the number of strange quarks per baryon in the particle population (where Q_{s_i} corresponds to the strangeness charge). Figure 12 shows f_s as a function of the radius for the most massive star provided by each parametrization. We have plotted the strangeness profiles only for the parametrizations that generate stars with masses of at least 1.99 $M_\odot$. As discussed above, lower values of the ζ parameter allow for the early appearance of hyperons in the star (i.e., outer layers). On the other hand, the growth of the hyperon content is slower for these cases (small ζ), providing a slightly lower central fraction of strangeness. We have computed the strangeness content only for the parametrizations in agreement with observational data, from which we conclude that the star's central values of strangeness do not depart much from $f_{s,c} = 0.65$, for a range of $\zeta = 0.040$–0.059. Finally, it is important to emphasize that all results concerning the ζ parameter are directly related to the effective mass of the nucleon and the compressibility modulus at saturation, as already discussed in Section 3.

5.2. The Role of The Hyperon Potentials on the Properties of Hyperon Stars

Although not much is known about hyperon–hyperon interactions, the hyperon–nucleon interactions are a little more constrained from hypernuclear data: the ΛN interaction has a well-constrained potential of about −28 MeV; the ΣN interaction points toward a repulsive potential; the ΞN interaction also presents an attractive potential, but not as well constrained as the ΛN.

Several works have investigated both attractive and repulsive U_Σ^N potentials (Knorren et al. 1995; Schaffner & Mishustin 1996; Mi et al. 2007; Schaffner-Bielich 2008; Negreiros et al. 2010; Vasconcellos et al. 2014) in the description of hadronic matter. In particular, we mention the analysis of the impact of different values of hyperon potentials on the properties of neutrons stars carried out by Weissenborn et al. (2012a) and also recently by Bhowmick et al. (2014), both using different RMF models. Following these works, in this subsection we aim to verify the effects of hyperon potentials in our model.

Initially, we vary U_Λ^N and U_Σ^N around ± 2 MeV and ± 20 MeV, respectively. Fixing the values of the remaining hyperon potential, we solve the TOV equations for different choices of the ζ parameter. From this case, no significant effect on the maximum mass and radius of the neutron stars are found. The results for our model agree with those found in Weissenborn et al. (2012a) and Bhowmick et al. (2014) for different RMF models.

We then varied the U_Ξ^N potential around ± 10 MeV, from which we found a relevant alteration of the maximum mass of the stars predicted by the model. Figure 13 shows the mass–radius relation for different U_Ξ^N potentials and choices of the ζ-parameter. The other hyperon potentials are fixed to

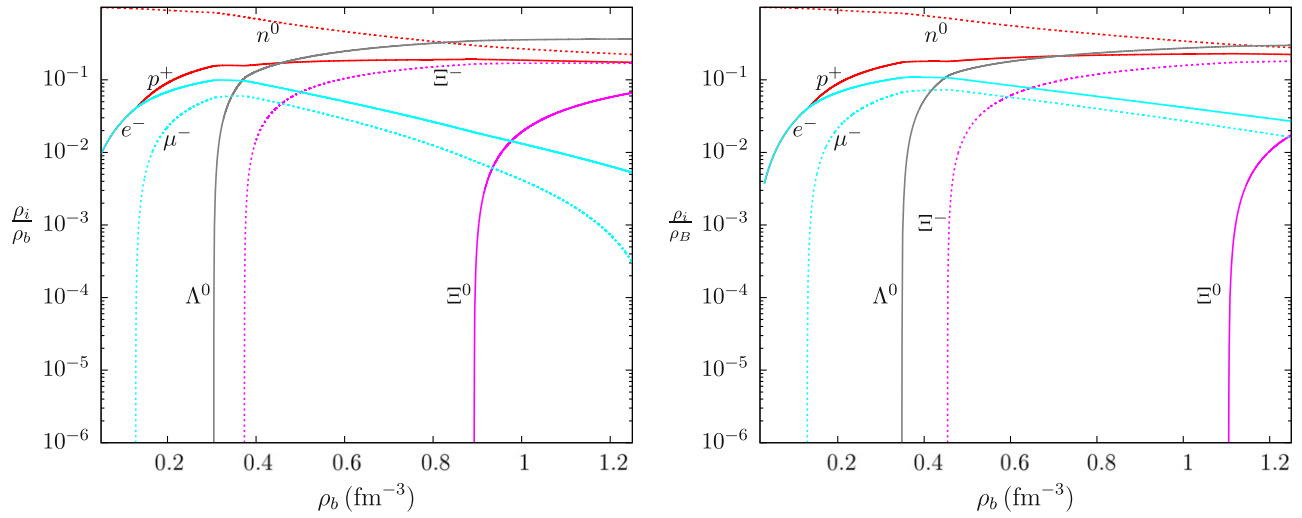

Figure 11. Particle population dependence on the parameter ζ. The left panel shows the population for $\zeta = 0.040$ and the right for $\zeta = 0.129$. The x-axis represents the baryon density and the y-axis the fraction of each particle specie normalized by the total baryon density.

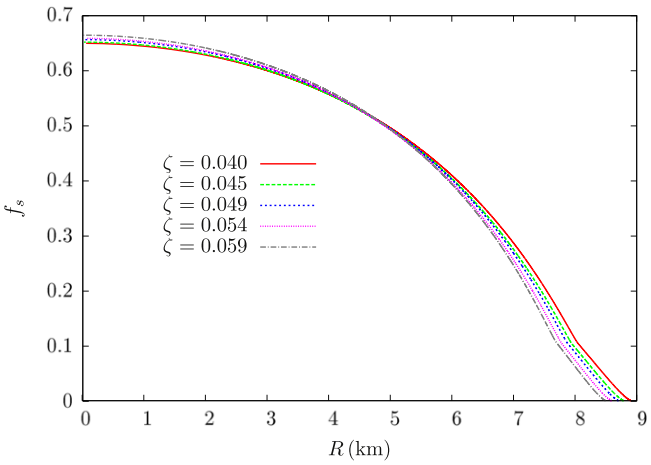

Figure 12. Fraction of strangeness f_s as a function of the radius for the maximum mass star provided for the ζ-parameter. The hyperon potentials are fixed to $U_\Lambda^N = -28$ MeV, $U_\Sigma^N = +30$ MeV, and $U_\Xi^N = -18$ MeV, and symmetry energy and its slope at saturation are $a_{\rm sym}^0 = 32$ MeV and $L_0 = 97$ MeV, respectively. We have plotted only the parametrizations that are in agreement with observational data.

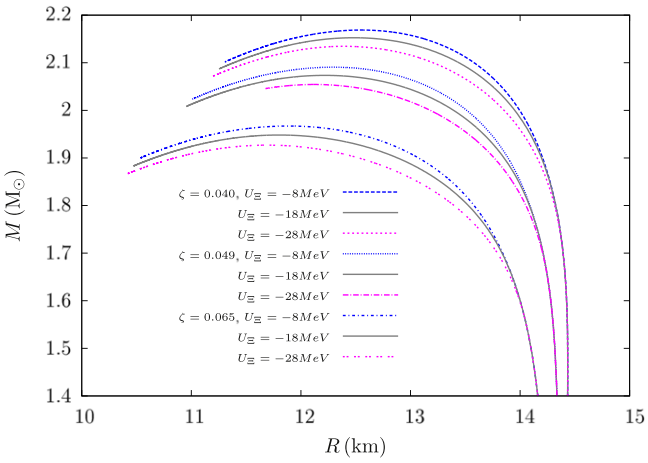

Figure 13. Mass–radius relation of hyperonic matter shown for different U_Ξ^N potentials and choices of ζ-parameter.

$U_\Lambda^N = -28$ MeV and $U_\Sigma^N = +30$ MeV, and the symmetry energy and its slope at saturation are $a_{\rm sym}^0 = 32$ MeV and $L_0 = 97$ MeV. The results presented here only include the three choices of the ζ parameter (0.040, 0.049, 0.065, corresponding to the higher, medium, and lower branches, respectively) that provide massive stars. We conclude that, for our model, a change of 10 MeV in the U_Ξ^N potentials results in a change of approximately 0.02 $M_\odot$ in the possible maximum masses of the stars.

From all of the star properties analyzed so far, we come to the conclusion that the ζ parameter and the U_Ξ^N potential are the only quantities that have a significant impact on the maximum star mass predicted by our model (in the $\sigma\omega\varrho\delta\phi$ version). For this reason, in Figure 14, we present the parameter space of these quantities related to the maximum mass of the stars. The vertical axis corresponds to the U_Ξ^N potential in the range of −3 to −48 MeV, the horizontal axis corresponds to the ζ parameter in a range of 0.040–0.071, and the scale of colors correspond to the stars's maximum mass (in $M_\odot$) provided by each choice of parameters. We indicate the limit of 1.97 $M_\odot$ that corresponds to the lower mass limit of the pulsar PSR J0348+0432.

The results in Figures 13 and 14 show that the maximum masses of the stars are higher as the attraction of the U_Ξ^N potential becomes weaker. Weak U_Ξ^N potentials shift the threshold of the Ξ's to higher densities, leaving hadronic matter to be populated mainly by $npe\mu\Lambda$ degrees of freedom at very high densities. In such a scenario, the filling of the energy states turns the EOS very stiff, which ultimately generates massive neutron stars. Note that the results in Figure 14, actually relate nuclear, hypernuclear and astrophysical data, since the ζ parameter has a direct relation with the effective mass of the nucleon and the compressibility modulus at saturation.

We now turn our attention to the effect of hyperon potentials on the strangeness content inside the stars. Since the U_Λ^N potential should not depart much from the value of −28 MeV from experimental data, we have verified the particle population of the model changing this value by ±2 MeV. In this case, no significant change was found.

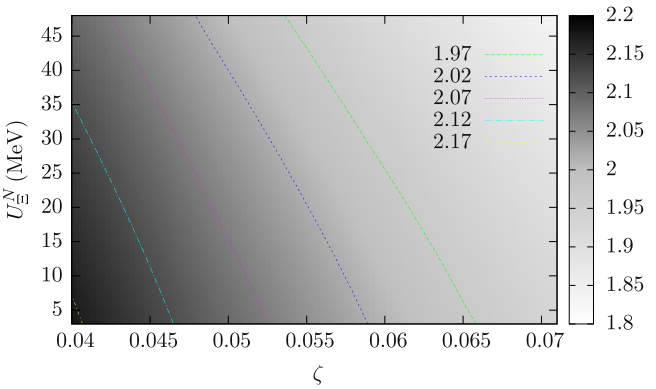

Figure 14. Parameter space related to the maximum star mass in the model. The horizontal and vertical axes correspond to the ζ parameter and the U_Ξ^N, respectively. The other hyperon potentials are fixed to $U_\Lambda^N = -28$ MeV and $U_\Sigma^N = +30$ MeV, and symmetry energy and its slope at saturation are $a_{\rm sym}^0 = 32$ MeV and $L_0 = 97$ MeV, respectively.

Figure 15 shows the particle population for different U_Σ^N potentials. The left panel corresponds to $U_\Sigma^N = +10$ MeV and the right one to $U_\Sigma^N = +50$ MeV, for $\zeta = 0.040$. The results show that the Σ^+ populate matter only at very high densities (0.86 fm^{-3}) in the case of a weak repulsion of $U_\Sigma^N = +10$ MeV. This result departs from the usual appearance of the Σ^- before of the Σ^+, which is due to the fact that, at these high densities, the charge neutrality is generated by the Ξ^-, with only small contributions from the leptons. Furthermore, the major contribution to the isospin density comes from the neutrons, which is the source term for the ϱ meson. As the Σ^+ has a strong attractive interaction via the ϱ meson, this hyperon appears at smaller densities than the Σ^-.

We report a threshold value of $U_\Sigma^N = +26$ MeV for the vanishing of Σ particles in our model in a range of $0 - 10\rho_0$ (for fixed $U_\Lambda^N = -28$ MeV and $U_\Xi^N = -18$ MeV), which does not depend on the ζ parameter. As Σ's appear only at very high densities, that usually exceed the central densities in neutron stars in certain models, the value of U_Σ^N does not bring important astrophysics predictions concerning neutron stars in those cases, as already pointed out by Schaffner (Schaffner-Bielich 2008).

The particle population for different U_Ξ^N potentials is shown in Figure 16, where the left and right panels correspond to $U_\Xi^N = -8$ MeV and $U_\Sigma^N = -28$ MeV, respectively, for $\zeta = 0.040$. It can be seen that an attractive U_Ξ^N potential, such as the one at the bottom panel, pulls the appearance of Ξ's to lower densities. Ultimately, a very strong attraction can reverse the order of appearance of the Λ and Ξ^- baryons. In particular, a difference of 20 MeV in the U_Ξ^N potential shifts the density threshold for the appearance of Ξ^- and Ξ^0 by about 0.07 fm^{-3} and 0.15 fm^{-3}, respectively.

Since different values of the U_Ξ^N potential significantly affect the hyperon population, in Figure 17 we investigate the strangeness content f_s (vertical axis) as a function of the radius of the maximum mass star reproduced (horizontal axis) for fixed $\zeta = 0.040$. The mass and central densities of the corresponding stars ranges from 2.09 $M_\odot$ and 0.90 fm^{-3} (for $U_\Xi^N = -48$ MeV) to 2.18 $M_\odot$ and 0.83 fm^{-3} (for $U_\Xi^N = -3$ MeV). The curves in Figure 17 indicate an increase in the fraction of strangeness as the attraction of the potential U_Ξ^N gets stronger. Strong attractive U_Ξ^N potentials shift the threshold of hyperons appearance to lower densities (higher radius), leaving a broader range of densities for f_s (hyperon population) to grow. Hence, the potentials that allow the appearance of hyperons at lower densities provide more strangeness at the center of the star. In particular, the range of -3 to -48 MeV for U_Ξ^N provides central values of f_s of about 0.62–0.74.

Note that, since varying U_Λ^N and U_Σ^N generate always the same family of stars, the f_s profile is not altered by the change of their values. Finally, we again stress that the hyperon potentials concerning the hyperon–nucleon (YN) interactions have no effect on the radius of neutron stars, in agreement with Weissenborn et al. (2012a) and Bhowmick et al. (2014). This result is not dependent on different choices of parameters of the model.

5.3. The Role of σ^* Meson on the Properties of Hyperon Stars

In order to introduce the remaining interaction between hyperons due to the meson σ^*, we vary the strengh of the coupling constant $g_{\sigma^* Y}$, setting $g_{\sigma^*\Lambda} = g_{\sigma^*\Sigma} = g_{\sigma^*\Xi}$. This approach allows us to constrain hyperon–hyperon interactions through astrophysical data investigation, differently from fixing a value of the hyperon–hyperon potential (U_Y^Y) (Schaffner & Mishustin 1996; Mi & You 2010).

To do so, we solve the TOV equations for coupling constants ranging $g_{\sigma^* Y} = 0$ to 5.0, as shown in Figure 18, for $\zeta = 0.040$. The results show that the σ^* meson has effects on both the maximum mass and the radius of the stars generated by the model. The increase of the σ^* coupling allows for more attraction in the matter, consequently lowering the maximum mass and radius predicted by the model.

In order to better quantify each effect, in Figure 19 we present the change in the radius of the canonical star of 1.4 $M_\odot$ as a function of the coupling $g_{\sigma^* Y}$. The choices of the parameter ζ are those which, in the absence of the σ^* meson, reach the minimum star mass value of 1.97 $M_\odot$. In particular, paying attention to the parametrization that provides the higher neutron star mass ($\zeta = 0.040$), we verify that, for a range $g_{\sigma^* Y} = 0 - 5.5$, the radius of the canonical star decreases by 0.52 km and the maximum mass drops from 2.15 $M_\odot$ to 2.12 $M_\odot$. It is important to note that the value of the coupling $g_{\sigma^* Y}$ cannot be simply increased, since it has a direct impact on the effective mass of the baryons. As already pointed out in the literature, at the density in which the effective masses of baryons reaches a zero value, it is necessary to use a formalism beyond mean field approximation and purely baryonic matter (Schaffner & Mishustin 1996; Taurines et al. 2001).

Analogously to the analysis carried out for the U_Ξ^N potential, in Figure 20 we present the parameter space concerning the $g_{\sigma^* Y}$ coupling, the ζ parameter (related to m_N^* and K_0), and the maximum mass of stars produced by our model. As already discussed above, the lower values of $g_{\sigma^* Y}$ and ζ are those that provide the highest star masses, as shown in the bottom left region of the plot. The threshold of the possible minimum mass is traced by the 1.97 $M_\odot$ curve, according to astrophysical data.

We also analyze the effect of the $g_{\sigma^* Y}$ coupling on the particle population in Figure 21. The left and right panels show

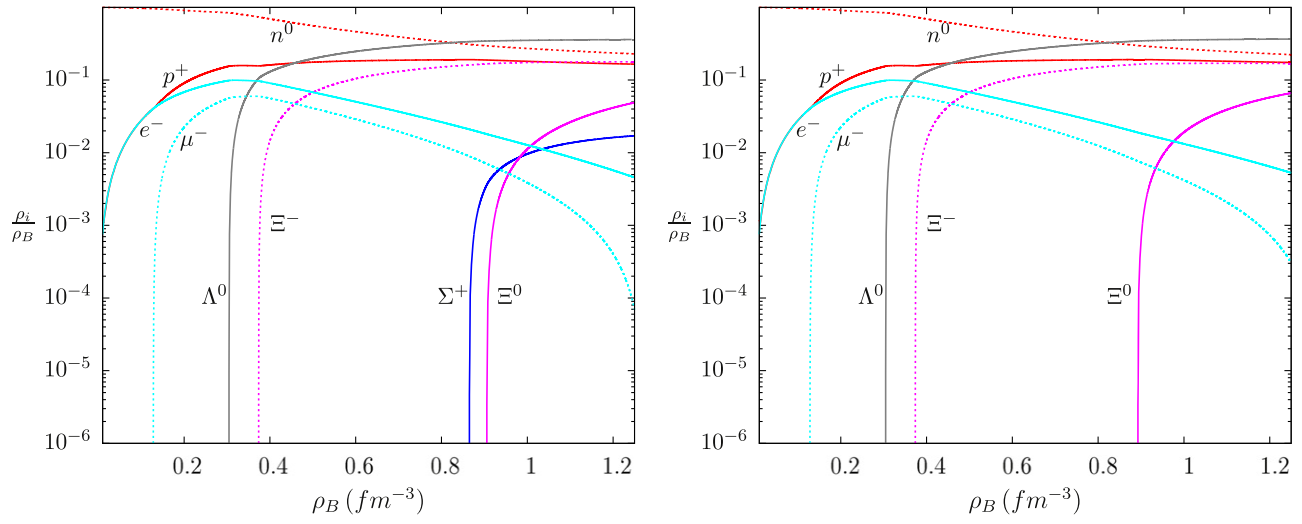

Figure 15. Particle population, for $\zeta = 0.040$, dependence on the hyperon potential U_Λ. The left and right panels correspond respectively to the cases of $U_\Sigma^N = +10$ MeV and $U_\Sigma^N = +50$ MeV. The other hyperon potential are fixed to $U_\Lambda^N = -28$ MeV and $U_\Xi^N = -18$ MeV.

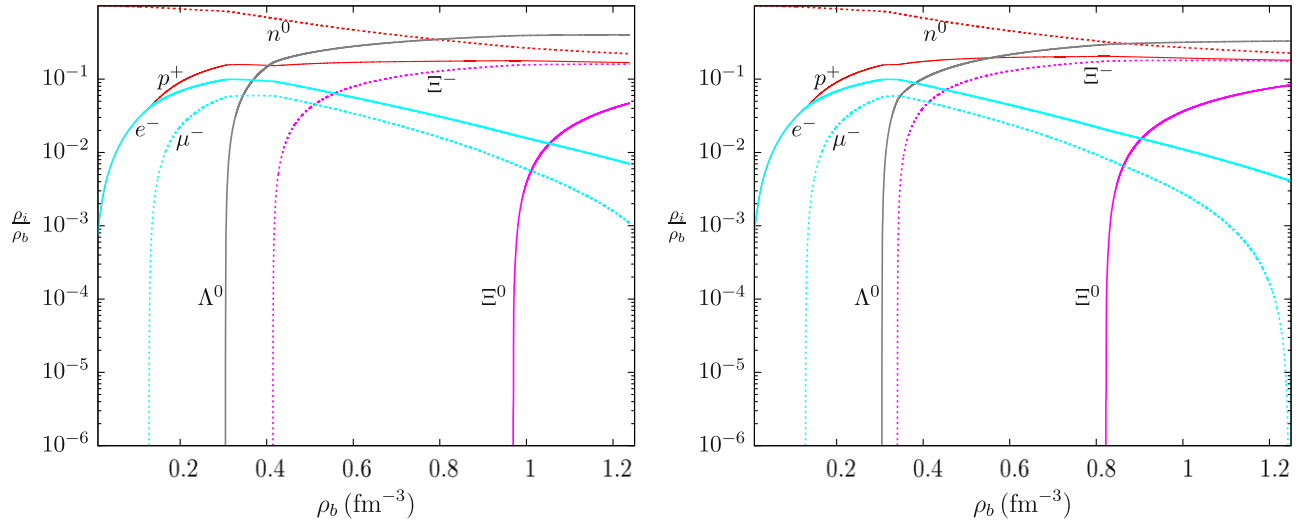

Figure 16. Same as Figure 15, but U_Λ, left and right panels correspond, respectively, to the cases of $U_\Xi^N = -8$ MeV and $U_\Xi^N = -28$ MeV.

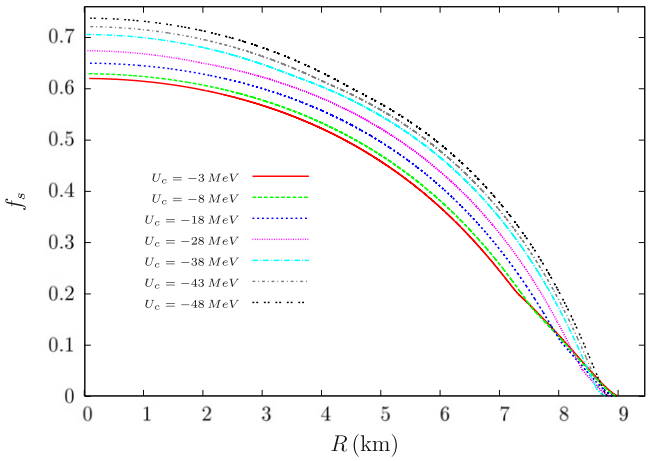

Figure 17. Fraction of strangeness f_s as a function of radius of the maximum mass star provided by $\zeta = 0.040$ for different choices of the U_Ξ^N potential. The other hyperon potentials are fixed to $U_\Lambda^N = -28$ MeV and $U_\Sigma^N = +30$ MeV, and symmetry energy and its slope at saturation are $a_{\rm sym}^0 = 32$ MeV and $L_0 = 97$ MeV, respectively.

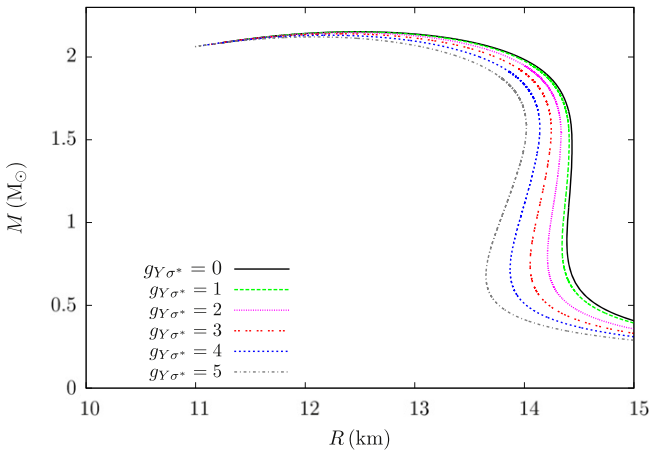

Figure 18. Mass–radius relation of hyperonic matter, for $\zeta = 0.040$, shown for different choices of $g_{\sigma^* Y}$ coupling constants. The hyperon potentials are fixed to $U_\Lambda^N = -28$ MeV, $U_\Sigma^N = +30$ MeV, and $U_\Xi^N = -18$ MeV, and symmetry energy and its slope at saturation are $a_{\rm sym}^0 = 32$ MeV and $L_0 = 97$ MeV, respectively.

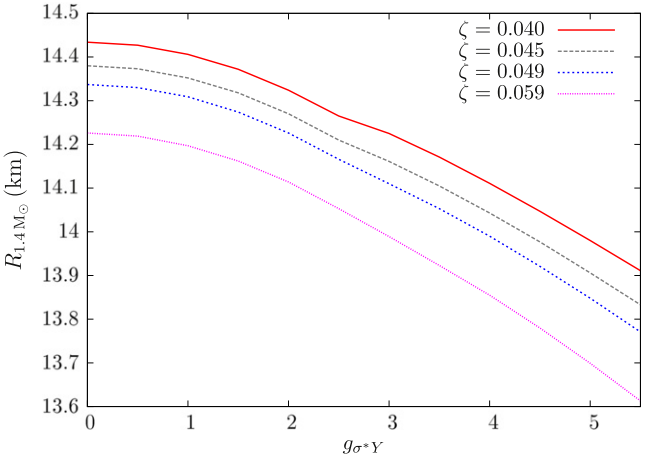

Figure 19. Radius of the 1.4 $M_\odot$ star dependence on the intensity of the $g_{\sigma^* Y}$ coupling costants, for different choices of the ζ parameter. The hyperon potentials are fixed to $U_\Lambda^N = -28$ MeV, $U_\Sigma^N = +30$ MeV, and $U_\Xi^N = -18$ MeV, and symmetry energy and its slope at saturation are $a_{\rm sym}^0 = 32$ MeV and $L_0 = 97$ MeV, respectively.

the population in the absence of the σ^* meson and the case in which $g_{\sigma^* Y} = 5.0$ (for $\zeta = 0.040$). The $g_{\sigma^* Y}$ coupling has impact only on the particle population at high densities, shifting the threshold of appearance of Ξ^0 to lower densities (from about 0.9 to 0.82 fm^{-3}).

More dramatically, the extra attraction introduced by the σ^* meson pushes the Σ^+ hyperon threshold back to the range of densities between 0 and $10\rho_0$. In particular, for $g_{\sigma^* Y} = 5.0$, these particles appear at 1.15 fm^{-3}, which cannot quite be reached in neutron stars. Moreover, as such high densities are only reached in the core of neutron stars, we also verified that the $g_{\sigma^* Y}$ coupling does not have significant effects on the strangeness profile of the stars.

Finally, we show in Table 6 the change in the values of the hyperon–hyperon potetials due to the introduction of the σ^* meson with a coupling $g_{\sigma^* Y}$. In the second column we show the nucleon–nucleon potential U_N^N that becomes less attractive for higher values of the ζ parameter, changing from −66.90 MeV for $\zeta = 0.040$ to −64.47 MeV for $\zeta = 0.059$. The value of U_N^N continues decreasing for higher values of ζ, reaching −59.56 MeV for $\zeta = 0.129$, which corresponds to the limiting value to reproduce the properties of nuclear matter at saturation density.

The introduction of the σ^* meson produces a stronger attraction among the Λ particles, changing U_Λ^Λ from +4.54 to −20.86 MeV for ζ and from −2.58 to −27.23 MeV for $\zeta = 0.059$. Like the nucleon–nucleon potential, the value of U_Λ^Λ continues to decrease for higher values of ζ, reaching −14.86 MeV (for $g_{\sigma^* Y} = 0$) and −38.19 MeV (for $g_{\sigma^* Y} = 5$), for $\zeta = 0.129$. All the other hyperons present repulsive interactions, even with the extra attraction introduced by the σ^* meson. Although the only measurement of the double-Λ hypernuclei points toward a weak $\Lambda\Lambda$ depth potential (Millener et al. 1988), only more hypernuclear data will be able to better constrain the σ^* coupling constants. The same applies to the other YY potentials, from which, so far, no accurate experimental data exist.

5.4. The Radius of the Canonical Star

Thus far in this paper we have investigated the effects of the parameters of the formalism on the properties of neutron stars, except the radius. Since most measured neutron star masses are clustered around 1.4 $M_\odot$, we now study all quantities that have impact on the radius of these stars.

We have discussed in previous sections that the parameter ζ, which relates the effective mass of the nucleon to the compressibility modulus at saturation, alters both the mass and the radius of compact stars. As already explained, ζ reflects how the many-body forces influence nuclear matter. In Section 4 we have shown that this parameter has an impact on the behavior of star matter properties at high densities, such as the density dependence of the compressibility modulus, symmetry energy, and its slope.

Lopes & Menezes (2014a) showed how an arbitrary variation of the slope L_0 changes the radius of the canonical star. In the particular case of our model, we verify that the only quantities that affect the behavior of the symmetry energy $a_{\rm sym}$ and its slope L at high densities are the ζ parameter and the constraints of these values ($a_{\rm sym}^0$ and L_0) at saturation. From this, we conclude that in our case the variation of the slope L_0 with respect to different densities, would arise from different behavior of many-body forces, for fixed values of $a_{\rm sym}^0$ and L_0.

Figure 22 shows the change of the radius of the canonical star as a function of the ζ parameter. Again, we stress that the change of the radius is directly related to the values of the effective mass and the compressibility modulus at saturation in this model. We observe that, for the range of values that fits nuclear data, the radius of the star changes about 0.8 km, but when we impose the observational limit of 1.97 $M_\odot$ (corresponding to the parametrization $\zeta = 0.04$–0.059), this value drops to 0.2 km.

Since the values of the symmetry energy and its slope also alter the radius of the stars, in Table 7 we quantify changes on the radius considering uncertainties in these values. Also, as the ζ parameter was shown to also affect the radius of neutron stars, we show these changes on the radius for the three parametrizations $\zeta = 0.040, 0.049, 0.059$.

For a 1.4 $M_\odot$ star that belongs to the family that predicts at least 1.97 $M_\odot$ maximum mass stars, we find that the smallest radius is 13.725 km, for the parametrization $\zeta = 0.059$, $a_{\rm sym} = 32$ MeV, $L_0 = 94$ MeV, and $g_{\sigma^* Y} = 4.0$. Relaxing the values of the asymmetry properties at saturation, the smallest radius of the 1.4 $M_\odot$ star drops to 13.54 km, for the parametrization $\zeta = 0.059$, $a_{\rm sym} = 29$ MeV, $L_0 = 85$ MeV, and $g_{\sigma^* Y} = 5.2$. Note that, although smaller values of $a_{\rm sym}$ increase the radius of the stars for fixed values of slope L_0, these smaller values of $a_{\rm sym}$ also allow for smaller values of L_0 (as already shown in Figures2–4) and, thus, smaller radii.

6. SUMMARY AND CONCLUSIONS

Substantial efforts have been made to determine the behavior of nuclear matter at high densities. Recent observations of massive neutron stars have renewed the interest in such studies. Given these massive stars, it has been suggested that hyperonic matter might not exist in compact stars, due to a possible excessive softnening of the EOS caused by these new degrees of freedom. Moreover, the comparison between the radius of nucleonic and hyperon stars predicted by several models has been reviewed, indicating that the radius of hyperon stars is

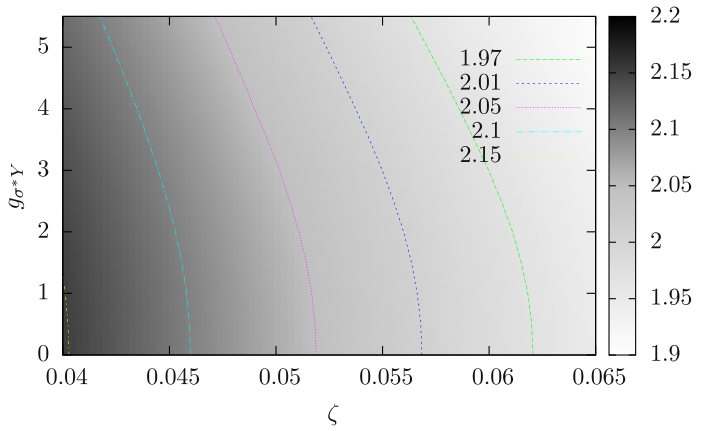

Figure 20. Parameter space related to star's maximum masses in the model. The horizontal and vertical axes correspond to the ζ parameter and $g_{\sigma^* Y}$, respectively. The hyperon potentials are fixed to $U_\Lambda^N = -28$ MeV, $U_\Sigma^N = +30$ MeV, $U_\Xi^N = -18$ MeV, and symmetry energy and its slope at saturation are $a_{\rm sym}^0 = 32$ MeV and $L_0 = 97$ MeV, respectively.

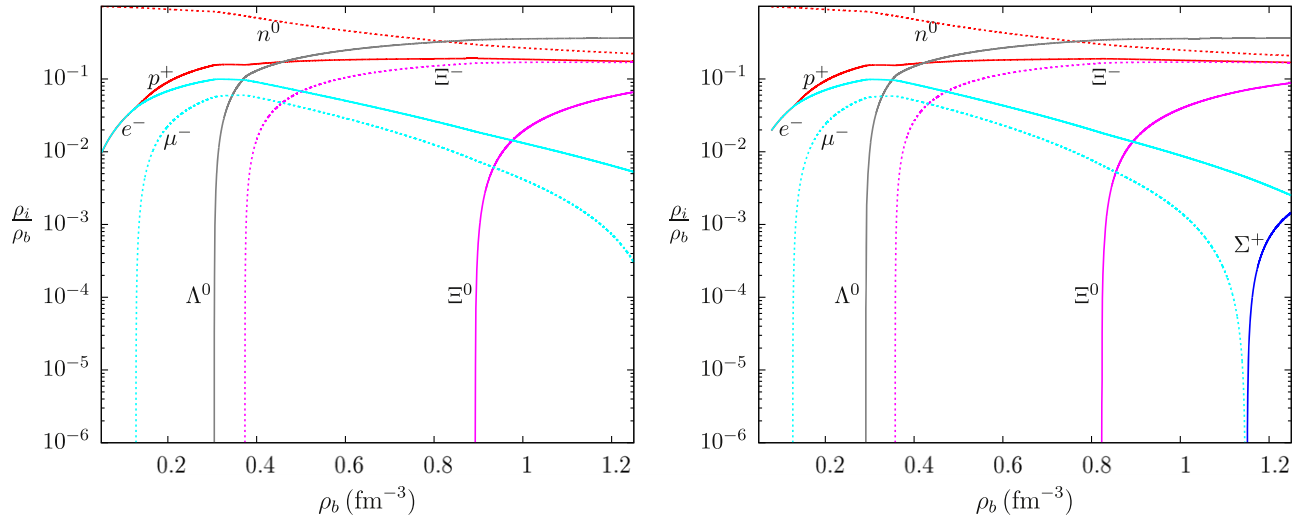

Figure 21. Particle population, for $\zeta = 0.040$, with $g_{\sigma^* Y} = 0$ (left panel) and $g_{\sigma^* Y} = 5$ (right panel) coupling strenghts. The hyperon potentials are fixed to $U_\Lambda^N = -28$ MeV, $U_\Sigma^N = +30$ MeV, and $U_\Xi^N = -18$ MeV and the symmetry energy and its slope are $a_{\rm sym}^0 = 32$ MeV and $L_0 = 97$ MeV.

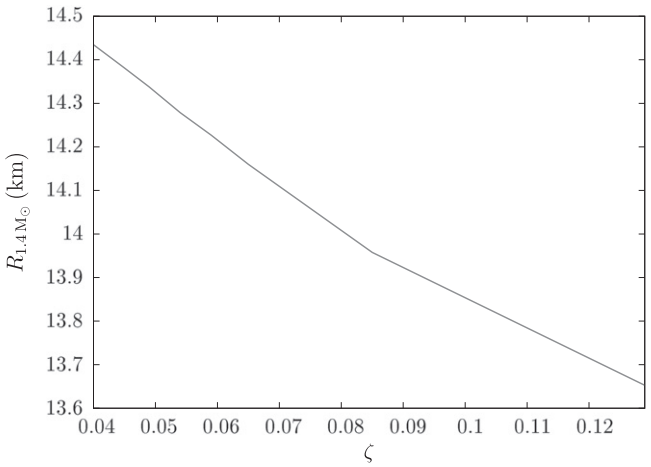

Figure 22. Effect on the ζ parameter on the radius of the canonical star ($1.4\,M_\odot$). The horizontal and vertical axes refer to the ζ parameter and the radius of the star, respectively. The hyperon potentials are fixed to $U_\Lambda^N = -28$ MeV, $U_\Sigma^N = +30$ MeV, $U_\Xi^N = -18$ MeV and symmetry energy and its slope at saturation are $a_{\rm sym}^0 = 32$ MeV and $L_0 = 97$ MeV, respectively.

substantialy larger than models fitted for nucleonic matter only (Fortin et al. 2014). In this work we extended the formalism proposed by Taurines et al. (2001) in order to describe hyperon stars. In the light of this extended model, we succeeded in describing neutron stars that agree with recent observations, despite the fact that it contains a considerable amount of hyperonic matter.

We have developed a new class of EOSs that allows for the presence of hyperons, and in which the baryon interactions are mediated by mesonic fields in a parametric derivative coupling. We extended the original version of the model by considering the complete set of scalar–isoscalar (σ, σ^*), vector–isoscalar (ω, ϕ), vector–isovector (ϱ), and scalar–isovector (δ) meson fields. We introduced the δ, σ^*, and ϕ mesons, since the first allows for a better extrapolation to asymmetric matter and the last two mesons play an important role in the description of hyperon interactions.

This approach allowed us to take nuclear medium effects into account, as the derivative coupling introduces an analogy to many-body forces, characterized by a single (ζ) parameter.

Table 6
Hyperon–Hyperon Potentials for Different Values of the ζ Parameter and g_{σ^*Y}

Hyperon potentials/ ζ	U_N^N (MeV)	U_Λ^Λ (MeV)	U_Σ^Λ (MeV)	U_Ξ^Λ (MeV)	U_Λ^Σ (MeV)	U_Σ^Σ (MeV)	U_Ξ^Σ (MeV)	U_Λ^Ξ (MeV)	U_Σ^Ξ (MeV)	U_Ξ^Ξ (MeV)
$\zeta = 0.040$, $g_{\sigma^*Y} = 0$	−66.90	+4.54	+46.25	+49.89	+41.54	+72.48	+69.13	+44.72	+67.92	+121.75
$\zeta = 0.040$, $g_{\sigma^*Y} = 5$	−66.90	−20.86	+20.53	+23.96	+15.10	+45.70	+42.12	+17.87	+40.70	+95
$\zeta = 0.049$, $g_{\sigma^*Y} = 0$	−65.79	+0.95	+43.25	+44.58	+38.27	+69.02	+64.03	+39.14	+62.87	+111.98
$\zeta = 0.049$, $g_{\sigma^*Y} = 5$	−65.79	−24.06	+17.85	+18.98	+12.13	+42.46	+37.24	+12.53	+35.83	+84.71
$\zeta = 0.059$, $g_{\sigma^*Y} = 0$	−64.47	−2.58	+40.36	+39.34	+35.14	+65.65	+59.06	+33.71	+58.01	+102.36
$\zeta = 0.059$, $g_{\sigma^*Y} = 5$	−64.47	−27.23	+15.26	+14.03	+9.25	+39.25	+32.44	+7.29	+31.10	+72.53

Note. The first column corresponds to the chosen parametrizations. In the second column we show the nucleon–nucleon potential refering to each parametrization. The third, fourth, and fifth columns show the corresponding values of the Λ, Σ, and Ξ potentials with respect to the Λ matter. The sixth, seventh, and eighth columns show the corresponding values of the Λ, Σ, and Ξ potentials with respect to the Σ matter. The ninth, tenth, and eleventh columns show the corresponding values of the Λ, Σ, and Ξ potentials with respect to the Ξ matter. the nucleon–hyperon potentials, the symmetry energy, and its slope at saturation are fixed to $U_\Lambda^N = -28$ MeV, $U_\Sigma^N = +30$ MeV, and $U_\Xi^N = -18$ MeV; $a_{\rm sym}^0 = 32$ MeV and $L_0 = 97$ MeV.

Table 7
Summary of the Properties That Affect Star Radii in the Model

$\Delta R_{1.4\,M_\odot}$	$\zeta = 0.040$	$\zeta = 0.049$	$\zeta = 0.059$
$[R_{1.4\,M_\odot}(L_0 = 110\ \mathrm{MeV}) - R_{1.4\,M_\odot}(L_0 = 97\ \mathrm{MeV})]$	0.33 km	0.35 km	0.37 km
$[R_{1.4\,M_\odot}(a^0_{\mathrm{sym}} = 30\ \mathrm{MeV}) - R_{1.4\,M_\odot}(a^0_{\mathrm{sym}} = 33\ \mathrm{MeV})]$	0.12 km	0.13 km	0.15 km
$[R_{1.4\,M_\odot}(g_{\sigma^*Y} = 0) - R_{1.4\,M_\odot}(g_{\sigma^*Y} = 5.5)]$	0.52 km	0.57 km	0.62 km

Note. The results are shown for hyperon stars for different parametrizations. The hyperon potentials are fixed to $U^N_\Lambda = -28$ MeV, $U^N_\Sigma = +30$ MeV, $U^N_\Xi = -18$ MeV and the symmetry energy, the slope of the symmetry energy, and the hyperon–hyperon coupling constant in relation to the σ^* meson are varied. In the first line, the symmetry energy is fixed to $a^0_{\mathrm{sym}} = 32$ MeV and $g_{\sigma^*Y} = 0$. In the second line, the slope of the symmetry energy is fixed to $L_0 = 101$ MeV and $g_{\sigma^*Y} = 0$. In the third line, the symmetry energy and its slope are fixed to $a^0_{\mathrm{sym}} = 32$ MeV and $L_0 = 97$ MeV. The results are shown only for the parametrizations in agreement with the observational data.

The many-body contributions were introduced as nonlinear terms contributions to the *effective coupling constants* of the model, whose effect is to turn them indirectly density dependent and also to lower the effective masses of the baryons. We also point out that, since the density dependence of the couplings comes from the scalar fields in this formalism, we avoid the rearrangement terms necessary in explicit density dependent formalisms (Typel & Wolter 1999).

The decrease of the coupling constants and the effective mass of the nucleon as a function of density has interesting phenomenological consequences, as it relates to the restoration of chiral symmetry and asymptotic freedom. However, an extensive analysis concerning this behavior must be carried out in detail in a future publication.

Each parametrization of the model generates a new EOS and, for particular parametrizations, it is possible to describe models already present in the literature such as Serot & Walecka (1986) and Zimanyi & Moszkowski (1990). Initially, we determined the connection between the ζ parameter and symmetric nuclear matter properties at saturation, from which we concluded that smaller values of the ζ parameter allows for lower (higher) nucleonic effective masses (compressibility modulus). In particular, we pointed out that the parameter ζ allows to determine both the effective mass of the nucleon and the compressibility modulus, differently from other models that need an extra parameter to fix these values (Boguta & Bodmer 1977; Typel & Wolter 1999).

We have also analyzed the parameter space that relates the symmetry energy a^0_{sym} and its slope L_0 to the coupling constants $g_{\varrho N}$ and $g_{\delta N}$ in order to determine the coupling constants of the isovector mesons to the nucleon at saturation density. Finally, we calculated the volume part of the isospin incompressibility and the skewness of the symmetry energy, from which we concluded that several parametrizations of the model are in good agreement with the tests carried out in the literature (Dutra et al. 2014).

Choosing the parameters according to nuclear matter saturation properties and the available hypernuclear data, we concluded that smaller values of ζ yield stiffer EOSs. We verified that different parametrizations also yield quantitatively different particle populations, but in all cases the hyperon population threshold density was kept at $\sim 2\rho_0$.

In order to further validate the microscopic model used, we compared macroscopic predictions with observed data. We calculated the mass–radius diagram for the parametrizations able to describe nuclear saturation properties. We have found that only the parametrizations with $0.040 \leqslant \zeta \leqslant 0.059$ were able to match recently observed masses of objects PSR J038+0432 ($M = 2.01 \pm 0.04 M_\odot$, (Antoniadis et al. 2013)) and PSR J1614-2230 ($M = 1.97 \pm 0.04 M_\odot$; Demorest et al. 2010), for fixed values of hyperon potentials. We have demonstrated that, since the value of the coupling constant $g_{\delta N}$ must remain small in order to ensure lower values of the slope L_0, the introduction of the δ meson does not have a strong effect on the maximum mass of the stars. On the other hand, we showed that the inclusion of the ϕ meson is crucial for the description of a $2\,M_\odot$ hyperon star.

Following previous works (Weissenborn et al. 2012a; Bhowmick et al. 2014), we have calculated the dependence of the star's observational properties on the hyperon potentials. Our results support those found in the literature, in which only the U^N_Ξ potential has a significant effect on the maximum mass of stars and, none of the hyperon potentials affect the radius of the stars. In order to find all quantities that modify star masses, we generated the parameter space that relates U^N_Ξ, ζ, and M_{max}, or hypernuclear, nuclear, and astrophysical observational data.

We carried out a similar analysis concerning the σ^* meson, from which a new parameter space, relating g_{σ^*Y}, ζ, and M_{max}, was generated. As far as we know, we report for the first time that nonzero values of the g_{σ^*Y} coupling decrease the radius of neutron stars significantly. We summarized the effects of all properties present in our model that modify the radius of the canonical star and we concluded that the many-body forces parameter contributes to the behavior of the nuclear asymmetric properties at high densities, which are reflected in the radii of these stars.

We must still make a final remark regarding the limitations of the formalism that we have developed and, most importantly, its uncertainties regarding the description of hyperon stars. First, we developed a model to describe nuclear matter at high densities by extrapolating the behavior of symmetric matter at saturation density to highly asymmetric matter at densities of about $8-10\rho_0$ (Schaffner & Mishustin 1996). Also, the introduction of hyperons in the system brings uncertainties related to the poor data from hypernuclear matter, such as the hyperon potentials, the assumption of a $SU(6)$ symmetry and the YY interacion concerning the σ^*(Fortin et al. 2014). There are works in the literature that consider approaches beyond $SU(6)$ (Mi et al. 2007; Lopes & Menezes 2014b; Weissenborn et al.

2012b) and the universality of $g_{\sigma^*\Lambda} = g_{\sigma^*\Xi} = g_{\sigma^*\Sigma}$ (Schaffner-Bielich & Gal 2000; Mi & You 2010; Gusakov et al. 2014). However, only new data will allow for a better understanding of hyperon matter at very high densities, for instance, from the possible measurements of multi-hyper nuclei such as those that will be provided by FAIR in the near future, and also from the analysis of hyperon–hyperon correlation in heavy-ion collisions (as originally proposed in Greiner & Muller 1989), and improved lattice QCD calculations of the YY potentials (Inoue et al. 2010).

Also, similarly, only new accurate observational data may provide reliable information regarding the radii of compact stars. Efforts in this direction have been made, mostly from the analysis of quiescent low-mass X-ray binaries (Guillot & Rutledge 2014; Lattimer & Steiner 2014). Still, there is a role played by different atmosphere modeling in these calculations, which provides a spectrum of results.

Our purpose with this study was to develop a new model for nuclear matter that takes into account nonlinear terms that simulate many-body forces and apply the formalism to describe hyperon stars in accordance with recent observations (Demorest et al. 2010; Antoniadis et al. 2013). A very straightforward extension of this work is the inclusion of nonlinear contributions to the coupling of isoscalar-vector and isovector-vector mesons, which requires a new analysis of saturation and asymmetric matter properties in the model. Also, in a future work, we plan to investigate the thermal evolution of such stars, which depends on their particle composition. Furthermore, we plan to investigate the phase transition to quark matter, which may take place in the core of high density neutron stars, and the effects of magnetic field on the microscopic and macroscopic properties of such stars. This work is already in progress.

R.O.G. and C.A.Z.V. would like to thank J. E. Horvath for the suggestion of the parameter space analysis. This work is partially supported by grant No. BEX 14116/13-8 of the PDSE CAPES and Science without Borders programs which are an initiative of the Brazilian Government. V.D. would like to acknowledge the support of HIC for FAIR and thank D. Menezes for her suggestions.

REFERENCES

Aguirre, R. 2001, PhRvC, 63, 025206
Aguirre, R., Civitarese, O., & de Paoli, A. 1996, NuPhA, 597, 543
Aguirre, R., & Schvellinger, M. 1997, PhRvC, arXiv:nucl-th/9704016
Ahn, J., Akikawa, H., Aoki, S., et al. 2013, PhRvC, 88, 014003
Antoniadis, J., Freire, P. C. C., Wex, N., et al. 2013, Sci, 340, 1233232
Banik, S., Hempel, M., & Bandyopadhyay, D. 2014, ApJS, 214, 22
Barranco, M., Lombard, R., Marcos, S., & Moszkowski, S. 1991, PhRvC, 44, 178
Bart, S., Chrien, R., Franklin, W., et al. 1999, PhRvL, 83, 5238
Bednarek, I., Haensel, P., Zdunik, J., Bejger, M., & Manka, R. 2012, A&A, 543, A157
Beringer, J., Arguin, J.-F., Barnett, R. M., et al. 2012, PhRvD, 86, 010001
Bhattacharyya, A., & Raha, S. 1996, PhRvC, 53, 522
Bhowmick, B., Bhattacharya, M., Bhattacharyya, A., & Gangopadhyay, G. 2014, PhRvC, 89, 065806
Biro, T., & Zimanyi, J. 1997, PhLB, 391, 1
Boguta, J., & Bodmer, A. 1977, NuPhA, 292, 413
Bonanno, L., & Sedrakian, A. 2012, A&A, 539, A16
Burigo, L., Bodmann, B., Jacobsen, R., Vasconcellos, C., & Fernandez, F. 2010, IJMPD, 19, 1563
Centelles, M., Roca-Maza, X., Vinas, X., & Warda, M. 2009, PhRvL, 102, 122502
Chen, L.-W. 2011, SCPMA, 54, 124
Chen, L.-W., Ko, C. M., & Li, B.-A. 2005a, PhRvL, 94, 032701
Chen, L.-W., Ko, C. M., & Li, B.-A. 2005b, PhRvC, 72, 064309
Chiapparini, M., Delfino, A., Malheiro, M., & Gattone, A. 1997, ZPhyA, 357, 47
Choudhury, S. K., & Rakshit, R. 1993, PhRvC, 48, 598
Cozma, M., Leifels, Y., Trautmann, W., Li, Q., & Russotto, P. 2013, PhRvC, 88, 044912
Delfino, A., Coelho, C., & Malheiro, M. 1995a, PhLB, 345, 361
Delfino, A., Coelho, C., & Malheiro, M. 1995b, PhRvC, 51, 2188
Demorest, P. B., Pennucci, T., Ransom, S. M., Roberts, M. S. E., & Hessels, J. W. T. 2010, Natur, 467, 1081
Dexheimer, V., & Schramm, S. 2008, ApJ, 683, 943
Dexheimer, V., Vasconcellos, C., & Bodmann, B. 2008, PhRvC, 77, 065803
Dover, C., & Gal, A. 1985, PrPNP, 12, 171
Duerr, H.-P. 1956, PhRv, 103, 469
Dutra, M., Lourenço, O., Avancini, S., et al. 2014, PhRvC, 90, 055203
Farine, M., Pearson, J., & Tondeur, F. 1997, NuPhA, 615, 135
Fortin, M., Zdunik, J., Haensel, P., & Bejger, M. 2014, arXiv:1408.3052
Friedman, E., & Gal, A. 2007, PhR, 452, 89
Fukuda, T., Higashi, A., Matsuyama, Y., et al. 1998, PhRvC, 58, 1306
Gal, A. 2005, NuPhA, 754, 91
Gal, A., & Millener, D. 2012, HyInt, 210, 77
Glendenning, N. 1982, PhLB, 114, 392
Glendenning, N. 1985, ApJ, 293, 470
Glendenning, N., & Moszkowski, S. 1991, PhRvL, 67, 2414
Glendenning, N., Weber, F., & Moszkowski, S. 1992, PhRvC, 45, 844
Gomes, R., Dexheimer, V., & Vasconcellos, C. 2014a, AN, 335, 666
Gomes, R., Dexheimer, V., & Vasconcellos, C. 2014b, in AIP Conf. Proc. 1595, The Role of Magnetic Fields in Hyperon Stars, ed. C. Spitaleri, L. Lamia, & R. G. Pizzone (New York, NY: AIP), 242
Greiner, C., & Muller, B. 1989, PhLB, 219, 199
Guillot, S., & Rutledge, R. E. 2014, ApJL, 796, L3
Gusakov, M., Haensel, P., & Kantor, E. 2014, MNRAS, 439, 318
Hanauske, M., Zschiesche, D., Pal, S., et al. 2000, ApJ, 537, 958
Hebeler, K., Lattimer, J., Pethick, C., & Schwenk, A. 2013, ApJ, 773, 11
Horowitz, C., Brown, E., Kim, Y., et al. 2014, JPhG, 41, 093001
Inoue, T., Ishii, N., Aoki, S., et al. 2010, PThPh, 124, 591
Jaminon, M., & Mahaux, C. 1989, PhRvC, 40, 354
Johnson, C., Horen, D., & Mahaux, C. 1987, PhRvC, 36, 2252
Johnson, M., & Teller, E. 1955, PhRv, 98, 783
Khan, E., & Margueron, J. 2013, PhRvC, 88, 034319
Khaustov, P., Alburger, D. E., Barnes, P. D., et al. 2000, PhRvC, 61, 054603
Knorren, R., Prakash, M., & Ellis, P. 1995, PhRvC, 52, 3470
Kubis, S., & Kutschera, M. 1997, PhLB, 399, 191
Kumar, R., Agrawal, B., & Dhiman, S. K. 2006, PhRvC, 74, 034323
Lastowiecki, R., Blaschke, D., Grigorian, H., & Typel, S. 2012, AcPPB, 5, 535
Lattimer, J. M., & Lim, Y. 2013, ApJ, 771, 51
Lattimer, J. M., & Prakash, M. 2005, PhRvL, 94, 111101
Lattimer, J. M., & Steiner, A. W. 2014, ApJ, 784, 123
Li, B.-A., & Han, X. 2013, PhLB, B727, 276
Li, T., Garg, U., Liu, Y., et al. 2007, PhRvL, 99, 162503
Liu, B., Greco, V., Baran, V., Colonna, M., & di Toro, M. 2002, PhRvC, 65, 045201
Lombard, R., Marcos, S., & Mares, J. 1995, PhRvC, 51, 1784
Lopes, L. L., & Menezes, D. P. 2014a, BrJPh, 44, 774
Lopes, L. L., & Menezes, D. P. 2014b, PhRvC, 89, 025805
Mares, J., Friedman, E., Gal, A., & Jennings, B. 1995, NuPhA, 594, 311
Marranghello, G. F., Providencia, C., & Santos, A. M. 2010, PhRvC, 81, 024307
Menezes, D., & Providencia, C. 2004, PhRvC, 70, 058801
Mi, A.-J., Li, A., & Zuo, W. 2007, ChPhy, 16, 3290
Mi, A.-J., & You, W. 2010, CoTPh, 53, 133
Millener, D., Dover, C., & Gal, A. 1988, PhRvC, 38, 2700
Miyazaki, K. 1994, PThPh, 91, 1271
Miyazaki, K. 1995, PThPh, 93, 137
Moszkowski, S. A. 1974, PhRvD, 9, 1613
Negreiros, R., Dexheimer, V., & Schramm, S. 2010, PhRvC, 82, 035803
Oppenheimer, J. R., & Volkoff, G. M. 1939, PhRv, 55, 374
Pal, S., Hanauske, M., Zakout, I., Stoecker, H., & Greiner, W. 1999, PhRvC, 60, 015802
Razeira, M., Mesquita, A., Vasconcellos, C. A., et al. 2011, IJMPE, 20, 146
Sahakian, G., & Vartanian, Y. 1963, Nuovo Cimento, 30, 82

Schaffner, J., Dover, C. B., Gal, A., et al. 1994, AnPhy, 235, 35
Schaffner, J., & Mishustin, I. N. 1996, PhRvC, 53, 1416
Schaffner, J., Stoecker, H., & Greiner, C. 1992, PhRvC, 46, 322
Schaffner-Bielich, J. 2008, NuPhA, 804, 309
Schaffner-Bielich, J., & Gal, A. 2000, PhRvC, 62, 034311
Schaffner-Bielich, J., Hanauske, M., Stoecker, H., & Greiner, W. 2002, PhRvL, 89, 171101
Serot, B. D., & Walecka, J. D. 1986, Advances in Nuclear Physics, Vol. 16 (New York: Plenum)
Sotani, H., Iida, K., & Oyamatsu, K. 2015, PhRvC, 91, 015805
Steiner, A., & Gandolfi, S. 2012, PhRvL, 108, 081102
Steiner, A. W., Lattimer, J. M., & Brown, E. F. 2010, ApJ, 722, 33
Stone, J., Stone, N., & Moszkowski, S. 2014, PhRvC, 89, 044316
Sugahara, Y., & Toki, H. 1994, NuPhA, A579, 557
Takahashi, H., Ahn, J., Akikawa, H., et al. 2001, PhRvL, 87, 212502
Taurines, A., Vasconcellos, C., Malheiro, M., & Chiapparini, M. 2001, PhRvC, 63, 065801
Todd-Rutel, B., & Piekarewicz, J. 2005, PhRvL, 95, 122501
Toki, H., Hirata, D., Sagahara, Y., Sumiyoshi, K., & Tanihata, I. 1995, NuPhA, 588, 357
Tolman, R. C. 1939, PhRv, 55, 364
Tsang, M., Stone, J., Camera, F., et al. 2012, PhRvC, 86, 015803
Typel, S., & Wolter, H. 1999, NuPhA, 656, 331
van Dalen, E., Colucci, G., & Sedrakian, A. 2014, PhLB, 734, 383
Vasconcellos, C., Gomes, R., Dexheimer, V., et al. 2014, AN, 335, 763
Wang, Y., Guo, C., Li, Q., et al. 2014, PhRvC, 89, 044603
Weisberg, J. M., & Taylor, J. H. 2005, in ASP Conf. Ser. 328, The Relativistic Binary Pulsar B1913+16: Thirty Years of Observations and Analysis, ed. F. A. Rasio & I. H. Stairs (San Francisco, CA: ASP), 25
Weissenborn, S., Chatterjee, D., & Schaffner-Bielich, J. 2012a, NuPhA, 881, 62
Weissenborn, S., Chatterjee, D., & Schaffner-Bielich, J. 2012b, PhRvC, 85, 065802
Yamamoto, Y., Furumoto, T., Yasutake, N., & Rijken, T. A. 2014, PhRvC, 90, 045805
Zimanyi, J., & Moszkowski, S. 1990, PhRvC, 42, 1416